Corrosivity of Water-Soluble Sulfate Ions in Simulated Pore Water Solutions and Different Types of Grout Samples

PUBLICATION NO. FHWA-HRT-21-052

MAY 2021

U.S. Department of Transportation
Federal Highway Administration

Research, Development, and Technology
Turner-Fairbank Highway Research Center
6300 Georgetown Pike
McLean, VA 22101-2296

FOREWORD

This final report presents research findings of an accelerated corrosion test program to determine the corrosivity of water-soluble sulfate ions in the simulated grout pore water and how these ions are present in various types of grout samples. The research product can enhance the bridge owners' understanding of sulfate-induced corrosion in the grouted post-tensioned tendons and help their management of prestressed concrete bridges containing this type of tendons. This report is expected to be of interest to bridge program personnel from Federal, State, and local transportation departments as well as to parties engaged in bridge-related research.

Cheryl Allen Richter, P.E., Ph.D.
Director, Office of Infrastructure
Research and Development

TECHNICAL REPORT DOCUMENTATION PAGE

1. Report No. FHWA-HRT-21-052	2. Government Accession No.	3. Recipient's Catalog No.
4. Title and Subtitle Corrosivity of Water-Soluble Sulfate Ions in Simulated Pore Water Solutions and Different Types of Grout Samples		5. Report Date May 2021 6. Performing Organization Code
7. Author(s) Seung-Kyoung Lee (ORCID ID 0000-0001-7367-5197)		8. Performing Organization Report No.
9. Performing Organization Name and Address SK Lee & Associates, Inc. 10813 Fieldwood Drive Fairfax, VA, 22030 Appendix prepared by Wiss, Janney, Elstner Associates, Inc. 330 Pfingsten Road Northbrook, IL 60062		10. Work Unit No. 11. Contract or Grant No. DTFH6112D00030T13001; DTFH6117D00017
12. Sponsoring Agency Name and Address Office of Infrastructure Research and Development Federal Highway Administration 6300 Georgetown Pike McLean, VA 22101		13. Type of Report and Period Covered Final Report; July 2014–November 2020 14. Sponsoring Agency Code HRDI-30

15. Supplementary Notes
The Technical Contact was Frank Jalinoos (HRDI-30) and the Contracting Officer's Representative was Cara Fitzgerald (HRDI-1).

16. Abstract
While sulfate-induced corrosion problems have been observed in segregated grout, the existing literature lacks useful information about the role of sulfate ions in the corrosion process. To produce empirical data on the corrosivity and concentration of water-soluble sulfate ions under different grout conditions, researchers performed a laboratory study. In low-pH aqueous solutions, simulating carbonated bleed water and grout pore water, water-soluble sulfate ions were as detrimental as chloride to post-tensioned (PT) strands if the strands were not protected by high-pH grout. In high-pH aqueous solutions, sulfate was less corrosive than chloride. When chloride and sulfate of equal concentrations coexisted in different pH aqueous solutions, chloride was the dominant species in determining corrosivity of the solutions. Like chloride ions, water-soluble sulfate ions showed temperature-dependent corrosivity in that corrosion was more severe at the elevated than ambient temperature. Mean corrosion rates at the near-freezing temperature were less than 10 percent of those measured at the ambient temperature, regardless of sulfate concentration. The content of water-soluble sulfate in raw grout powders ranged from 0.35 to 1.0 percent by weight of sample, but most of the sulfate became bound to the hardened grout and the water-soluble sulfate reduced to 0.1 percent. Aged/expired raw grout was more prone to segregation and readily released water-soluble sulfate ions into the segregated grout. Petrographic examination and chemical analyses revealed that pore water and soft/wet segregated grout retained 100 times the water-soluble sulfate and more than five times the total sulfur content than dried and hardened grout did. This is because water-soluble sulfate ions can migrate via water movement toward areas with more moisture. If the segregated grout maintains a low-pH environment by carbonation, corrosion can be initiated on a strand in direct contact with a carbonated layer of segregated grout with a concentration of water-soluble sulfate ions as low as 0.05 percent by weight of sample. Just a thin film of carbonation, in intimate contact with the steel, is sufficient to induce the intensive corrosion.

17. Key Words	18. Distribution Statement
Corrosion, galvanic corrosion, pitting corrosion, electrochemical test, carbonation, sulfates, cement grouts	No restrictions. This document is available to the public through the National Technical Information Service, Springfield, VA 22161. http://www.ntis.gov

19. Security Classif. (of this report)	20. Security Classif. (of this page)	21. No. of Pages	22. Price
Unclassified	Unclassified	74	N/A

Form DOT F 1700.7 (8-72) Reproduction of completed page authorized.

SI* (MODERN METRIC) CONVERSION FACTORS

APPROXIMATE CONVERSIONS TO SI UNITS

Symbol	When You Know	Multiply By	To Find	Symbol
		LENGTH		
in	inches	25.4	millimeters	mm
ft	feet	0.305	meters	m
yd	yards	0.914	meters	m
mi	miles	1.61	kilometers	km
		AREA		
in^2	square inches	645.2	square millimeters	mm^2
ft^2	square feet	0.093	square meters	m^2
yd^2	square yard	0.836	square meters	m^2
ac	acres	0.405	hectares	ha
mi^2	square miles	2.59	square kilometers	km^2
		VOLUME		
fl oz	fluid ounces	29.57	milliliters	mL
gal	gallons	3.785	liters	L
ft^3	cubic feet	0.028	cubic meters	m^3
yd^3	cubic yards	0.765	cubic meters	m^3
		NOTE: volumes greater than 1,000 L shall be shown in m^3		
		MASS		
oz	ounces	28.35	grams	g
lb	pounds	0.454	kilograms	kg
T	short tons (2,000 lb)	0.907	megagrams (or "metric ton")	Mg (or "t")
		TEMPERATURE (exact degrees)		
°F	Fahrenheit	5 (F-32)/9 or (F-32)/1.8	Celsius	°C
		ILLUMINATION		
fc	foot-candles	10.76	lux	lx
fl	foot-Lamberts	3.426	candela/m^2	cd/m^2
		FORCE and PRESSURE or STRESS		
lbf	poundforce	4.45	newtons	N
lbf/in^2	poundforce per square inch	6.89	kilopascals	kPa

APPROXIMATE CONVERSIONS FROM SI UNITS

Symbol	When You Know	Multiply By	To Find	Symbol
		LENGTH		
mm	millimeters	0.039	inches	in
m	meters	3.28	feet	ft
m	meters	1.09	yards	yd
km	kilometers	0.621	miles	mi
		AREA		
mm^2	square millimeters	0.0016	square inches	in^2
m^2	square meters	10.764	square feet	ft^2
m^2	square meters	1.195	square yards	yd^2
ha	hectares	2.47	acres	ac
km^2	square kilometers	0.386	square miles	mi^2
		VOLUME		
mL	milliliters	0.034	fluid ounces	fl oz
L	liters	0.264	gallons	gal
m^3	cubic meters	35.314	cubic feet	ft^3
m^3	cubic meters	1.307	cubic yards	yd^3
		MASS		
g	grams	0.035	ounces	oz
kg	kilograms	2.202	pounds	lb
Mg (or "t")	megagrams (or "metric ton")	1.103	short tons (2,000 lb)	T
		TEMPERATURE (exact degrees)		
°C	Celsius	1.8C+32	Fahrenheit	°F
		ILLUMINATION		
lx	lux	0.0929	foot-candles	fc
cd/m^2	candela/m2	0.2919	foot-Lamberts	fl
		FORCE and PRESSURE or STRESS		
N	newtons	2.225	poundforce	lbf
kPa	kilopascals	0.145	poundforce per square inch	lbf/in^2

*SI is the symbol for International System of Units. Appropriate rounding should be made to comply with Section 4 of ASTM E380. (Revised March 2003)

TABLE OF CONTENTS

LIST OF FIGURES

LIST OF TABLES

LIST OF ABBREVIATIONS

Abbreviations

ASR	alkali–silica reaction
AV	air void
CE	counter electrode
CPP	cyclic potentiodynamic polarization
FDOT	Florida Department of Transportation
FHWA	Federal Highway Administration
GUTS	guaranteed ultimate tensile strength
IC	ion chromatography
LPR	linear polarization resistance
PT	post-tensioned
PTI	Post-Tensioning Institute
RE	reference electrode
SA	surface area
SDEV	standard deviation
SF	silica fume
WE	working electrode
XRD	X-ray diffraction

Measurements and Chemical Compounds

Ag/AgCl	silver/silver chloride
E_{corr}	corrosion potential
I_{corr}	corrosion current
i_{corr}	corrosion current density
ksi	kilopound per square inch
mpy	mils per year
NaCl	sodium chloride
Na_2SO_4	sodium sulfate
ppm	parts per million
R	resistance
R^2	coefficient of determination
SO_3	sulfur trioxide
SO_4^{2-}	sulfate ion

CHAPTER 1. INTRODUCTION

Since the 1970s, the number of pre-tensioned and post-tensioned (PT) concrete bridge structures utilizing high-strength seven-wire strands has increased steadily. In general, the durability of PT bridges in the United States has been considered very good. However, by the end of 2019, tendon corrosion problems had affected eight major PT bridges in five States.[(1–3)1]

In the past, grout segregation issues were reported occasionally, even after the introduction of prepackaged, high-performance grout products possessing zero-bleed and thixotropic characteristics in the early 2000s.

The first corrosion problem associated with segregated grout was reported in the United States in 2011, when two ruptured PT tendons were discovered in the Ringling Causeway Bridge in Sarasota, FL, one in January and the other in July. The tendons were approximately 7 yr old at the time of the failures and contained a prepackaged, commercial grout product. In-depth investigations carried out by the Florida Department of Transportation (FDOT) in the field and the laboratory linked segregated grout to the observed tendon failures. The grout segregation, which had developed in some high elevation tendon sections, was characterized as having a soft/wet plastic consistency (moisture content 50 to 80 percent), a sedimented silica fume (SF) layer, and a chalky appearance (moisture content 20 to 50 percent). The segregated grout was also reported to have other characteristics, including a high pH, high concentrations of sulfate and other soluble ions, and no significant chlorides. Based on the investigation results, FDOT concluded that the high level of free sulfate ions in the segregated grout was responsible for the premature corrosion problem or, at least, had been a major contributing factor.[(4–6)] Similar corrosion problems involving segregated grout in PT bridges were also encountered in other countries.

In Italy, an external tendon in an unidentified PT bridge failed prematurely less than 2 yr after construction (year of failure was not reported). Severe pitting corrosion of 27 seven-wire strands in contact with segregated grout was responsible for the tendon failure. The problematic grout had been mixed at the construction site with a water-to-cement ratio of 0.32 and a commercial admixture specifically for grouts.[(7)] Because the fresh grout mix had passed the inclined-tube test and the wick test, per the specifications of *EN 445: Grout for Prestressing Tendons – Test Methods*, grout segregation was not anticipated.[(8)] However, segregation was discovered in the inclined parts of the tendons between the last deviation points and the anchorages. The segregated grout was described as having a whitish, unhardened paste, similar to the soft/wet grout observed in the Ringling Bridge case. Severe pitting corrosion took place only on the strand sections in contact with the segregated grout. Chemical analysis of different types of grout samples revealed that the mean concentration of sulfates in terms of SO_3 in the segregated grout was 6.29 (maximum 7.88) percent by weight of sample, whereas chloride concentration was minimal.[(7,9)]

[1]Information from a forthcoming FHWA report entitled *Corrosion-Induced Durability Issues and Maintenance Strategies for Post-Tensioned Concrete Bridges*.

In 2016, the Seoul Metropolitan Facility Management Corporation discovered several failed external tendons on two precast segmental box girder bridges in South Korea. In one of the affected bridges, different forms of segregated grout containing excessive amounts of free sulfate ions were responsible for some of the severe corrosion damage. As in the cases described previously, the chloride concentration was below the threshold for corrosion.[10]

A segregated grout problem involving free sulfate ions was also encountered in a carefully controlled laboratory environment. In 2012, in response to nationwide chloride contamination of a prepackaged grout product, the Federal Highway Administration (FHWA) conducted an accelerated corrosion test study under the Long-Term Bridge Performance (LTBP) program to determine the chloride threshold for grouted PT tendons.[11,12] Some of the fabricated multistrand specimens exhibited a porous and black-particle-covered segregated grout layer at the grout and artificial void interfaces. During the autopsy, severe corrosion was observed at the interfaces of three specimens containing 0, 0.4, and 2.0 percent chloride by weight of cement. The discovery of severe corrosion in the 0 percent chloride specimen triggered a small-scale laboratory investigation using ion chromatography (IC) to quantify water-soluble sulfate concentrations in various grout samples, including the black particles scraped off the 0 percent chloride specimen. The raw grout powder contained 0.9 percent of water-soluble sulfate ions by weight of cement. The samples taken from the normally hardened grout contained negligible sulfate ions. However, the black particles and segregated grout layer samples collected from the 0 percent chloride specimen contained 2.7 percent of water-soluble sulfate ions by weight of cement. It was apparent that the segregation process had produced the excessive water-soluble sulfate ions in the segregated grout layer and had resulted in the observed corrosion damage.[12]

That unexpected finding led researchers to conceive a potential laboratory study to further investigate sulfate-related corrosion. The study was subsequently carried out in two phases: the first phase, in 2014, was conducted under the LTBP program; the second phase, in 2018, was conducted under the Coatings and Corrosion Laboratory research program.

In a separate research effort to develop a failure forecasting model for PT tendons containing deficient grout, researchers performed an accelerated corrosion study. The objective of the study was to investigate the propensity of strand corrosion in the presence of water-soluble sulfate ions under different testing conditions, including grout segregation, recharging water, temperature, and pH.[13] This study found that the segregated grout specimens exhibited lower mean grout resistance variation with time. Upon adding recharging water into the artificial grout voids, the specimens experienced little resistance change compared to normally hardened grout specimens under the same conditions. It was concluded that segregation of grout resulted in a more corrosive condition, indicated by higher macrocell corrosion current, in the low-pH (i.e., carbonated) environment than the normally hardened counterparts in the same environment.

This report presents empirical scientific data from the accelerated corrosion studies, including how much water-soluble sulfate can be liberated under different grout conditions, the corrosivity of water-soluble sulfate ions as a function of concentration, and the sulfate-induced corrosion mechanism in deficient (i.e., segregated) grout.

CHAPTER 2. OBJECTIVES AND SCOPE OF WORK

Researchers carried out a 6-mo accelerated laboratory corrosion study to investigate sources of water-soluble sulfate in various types of grout samples and to test the corrosivity of sulfate ions in simulated carbonated and uncarbonated grout pore solutions. Specifically, the study had the following three objectives:

- Investigate the electrochemical (corrosion) behaviors of center wires exposed to sulfate and chloride ions in high and low-pH aqueous solutions.
- Characterize the physical characteristics of various types of grout samples.
- Determine the total amounts of water-soluble sulfate ions in raw grout powder ingredients and hydrated grout samples.

The scope of the work consisted of the following three tasks:

- Task 1 investigated the electrochemical behaviors of unstressed and stressed center wires exposed to various aqueous test solutions, which simulated bleed water or grout pore water containing various levels of water-soluble sulfate ions in uncarbonated and carbonated conditions. Additional laboratory tests were carried out to determine the effects of different strand manufacturers and surface cleanliness on corrosion.
- Task 2 examined the physical characteristics of different types of grout specimens and their chemical compositions. This task also employed petrographic examination and chemical analyses.
- Task 3 determined the amounts of water-soluble sulfate ions in raw grout, normally hardened grout specimens made with the recommended water dosage, and simulated segregated grout specimens containing excessive water.

CHAPTER 3. EXPERIMENTAL PROCEDURE

This chapter introduces the materials, test variables, and evaluation methods used in the accelerated corrosion experiments.

MATERIALS

Seven-Wire Strands

The 270-ksi, low-relaxation, seven-wire bare strands, compliant with American Society for Testing and Materials (ASTM) standard *A416 Standard Specification for Low-Relaxation, Seven-Wire Steel Strand for Prestressed Concrete*, were acquired from three suppliers who were readily available to provide the strand materials.[14]

Approximately 1,000 ft of 0.6-inch seven-wire strand were acquired from Supplier A. The strand was delivered in two precut lengths of 5.5 and 6.5 ft. To prevent surface contamination during handling and transportation, each strand piece was delivered without removing its outer six wires. The center wires were extracted at the test facility and wrapped with large plastic sheets while in storage.

Approximately 200 ft of 0.5-inch strand from Supplier B were also acquired to compare the corrosion performance of two strand materials supplied by different vendors.

Another 50 pieces of 0.6-inch strand were acquired from Supplier C in a precut length of 24 inches to perform additional testing near the final stage of this study.

The primary testing was performed with the strand material acquired from Supplier A, and supplementary testing was performed with strands acquired from Suppliers B and C.

Post-Tensioning Institute Class C Grout

Researchers used three commercially available Post-Tensioning Institute (PTI) Class C prepackaged grout products. They are designated as Products 1, 2, and 3 in this report. Twenty 50-lb bags of Product 1 and 20 55-lb bags of Product 2 were acquired and used before their expiration dates.

All four bags of Product 3 were long expired, left over from research studies conducted in 2009 and 2012. In this report, the bags from 2009 are designated as #1 Old Product 3, and the bags from 2012 as #2 Old Product 3. While three of the #2 Old Product 3 bags had been kept in airtight pails, the fourth had been exposed to laboratory air and was labeled as the “opened bag.”

Although the expired Product 3 cannot be compared fairly against Products 1 and 2, researchers chose to test Product 3 to see if the results might offer valuable information about the adverse effects of expired grout, such as grout segregation and free sulfate content in raw grout and hardened grout samples.

TASK 1: ELECTROCHEMICAL TESTS OF CENTER WIRES

Researchers tested the extracted center wires in two batches (Batch #1 and Batch #2) using two popular electrochemical test methods: linear polarization resistance (LPR) to determine a wire's instantaneous rate of corrosion and cyclic potentiodynamic polarization (CPP) to characterize its pitting corrosion tendency.

The LPR tests employed four pH aqueous test solutions containing different concentrations of anions (sulfate and chloride). These solutions were intended to simulate the bleed water formed upon grout segregation or grout pore water in carbonated and uncarbonated conditions. The CPP tests measured the susceptibility of selected Batch #1 wires to pitting corrosion under different test conditions.

Experimental Setup

Batch #1 Testing

To complete testing of Batch #1, researchers carried out 568 electrochemical tests to compare the corrosivity of free sulfate ions against that of chloride ions dissolved in the test solutions.

Three pH test solutions were prepared by adding the chemicals listed in table 1 to commercially available distilled water (actual pH 7.8). All the test solutions were made at the ambient temperature in the laboratory. Plain distilled water was also employed as the fourth pH solution.

Table 1. Chemical compositions for three pH solutions.

Chemical Dissolved in 1 L of Distilled water	pH 10.0 (oz)	pH 12.5 (oz)	pH 13.6 (oz)
Calcium hydroxide	0	0.0071	0.0705
Sodium hydroxide	0.00014	0.0293	0.2928
Potassium hydroxide	0	0.0822	0.8219

The actual pH values determined using a digital pH meter were slightly different from the nominal values. The nominal pH is used throughout this report to distinguish pH groups 8.0 and 10.0 for carbonated conditions, and pH groups 12.5 and 13.6 for uncarbonated conditions.

At each pH, nine solutions containing five sulfate concentrations (0.2, 0.4, 0.8, 1.5, and 3.0 percent by weight of cement) and four chloride concentrations (0.08, 0.4, 0.8, and 2.0 percent by weight of cement) were prepared using sodium sulfate (Na_2SO_4) and sodium chloride (NaCl), respectively. The lowest chloride concentration—0.08 percent—was included based on the chloride limit specified in four sources.[15] A tenth anion-free solution was also prepared as a control. For the remainder of this report, anion concentrations are expressed without "by weight of cement," unless noted otherwise. A known cement weight of Product 3—67 percent of the bag weight—was used for all mix proportions. The other products were assumed to have similar ratios of cement. Distilled water was also used to investigate the corrosion behavior of PT strands in a contamination-free environment. Table 2 and table 3 list the recipes for the sulfate solutions and chloride solutions, respectively.

Table 2. Weight of Na_2SO_4 in test solutions.

Sulfate Concentration by Weight of Cement (Percent)	Na_2SO_4 in 33.8 fl oz of Distilled Water (oz)
0.2	0.278
0.4	0.556
0.8	1.112
1.5	2.085
3.0	4.170

Table 3. Weight of NaCl in test solutions.

Chloride Concentration by Weight of Cement (Percent)	NaCl in 33.8 fl oz of Distilled Water (oz)
0.08	0.124
0.4	0.619
0.8	1.239
2.0	3.098

Most of the LPR tests were performed at ambient (77 °F) and elevated temperatures (104 °F) to study the effect of temperature on the corrosivity of sulfate and chloride under different ionic concentrations. The remaining tests were performed in a walk-in environmental chamber at a nominal temperature of 32 °F. The chamber maintained an actual temperature of 40 °F.

A subset of the LPR specimens made with Supplier A strand was stressed at 60 percent of the guaranteed ultimate tensile strength (GUTS) to investigate the effect of stress on corrosion in each of the four pH solutions at two concentrations (0.4 and 0.8 percent) of sulfate ions and the same concentrations of chloride ions. Researchers also studied the effect that coexisting sulfate and chloride ions in a solution have on corrosion by using unstressed wires in four pH solutions at two equal concentrations (0.4 and 0.8 percent) of sulfate and chloride ions.

Strand producers are likely to apply lubricants and cleaning products to strand surfaces during the fabrication process. For the majority of the LPR tests, the uncleaned, as-received wires acquired from Supplier A were used after they were gently wiped with paper towels so that little of the factory-applied lubricant was removed. A different group of Supplier A strand and a second strand material acquired from Supplier B were cleaned before testing to determine whether the manufacturing process could influence the corrosion rate. To prepare the cleaned wires, the lubricant was chemically removed by wiping the wires several times with a rag soaked with denatured alcohol, followed by a final cleaning with a paper towel. The cleaned wires were tested in 0.4 and 0.8 percent sulfate solutions and in the same concentrations of chloride solutions. Duplicate or triplicate specimens were employed in most cases.

The stressed and unstressed center wires were vertically installed in the loading frames. Figure 1 through figure 3 show the experimental setups for Batch #1 at the ambient temperature, elevated temperature, and cold temperature, respectively. A heat lamp controlled by a digital thermometer ensured the elevated temperature remained at 104 °F.

Source: FHWA.

Figure 1. Photo. Ambient temperature test setup (77 °F) for Batch #1 with unstressed wires in the wooden frame and a stressed wire in the steel loading frame.

Source: FHWA.

Figure 2. Photo. Elevated temperature test setup (104 °F) for Batch #1.

Source: FHWA.

Figure 3. Photo. Cold temperature test setup (32 °F) for Batch #1 inside a walk-in environmental chamber.

Batch #2 Testing

To investigate the corrosivity of solutions with low sulfate concentrations (0.05, 0.10, and 0.15 percent), researchers carried out a second round of testing (Batch #2), as shown in figure 4 and figure 5. Another anion-free solution was prepared as a control. A total of 216 wire specimens were prepared for Batch #2 using the strands obtained from Supplier C.

Three wire specimens were employed for each test condition, in an unstressed and as-received surface condition only. All tests were performed at ambient (77 °F) and elevated temperatures (104 °F). As they did with Batch #1, researchers used four different pH solutions to test Batch #2. Again, the actual pH values were slightly different from the nominal values.

Unstressed, short center wires were placed vertically on the wooden platforms. The elevated temperature testing was conducted inside a commercial chest freezer. A heat lamp controlled by a digital thermometer maintained the temperature accurately at 104 °F.

Source: FHWA.

Figure 4. Photo. Ambient temperature test setup for Batch #2.

Source: FHWA.

Figure 5. Photo. Elevated temperature test setup for Batch #2.

Construction of Test Cells

Specially constructed test cells were prepared for accelerated corrosion testing. Each test cell was reusable and consisted of the following:

- A 6.8 fl oz transparent plastic cup with a paper lid.
- A center wire as a working electrode (WE).
- A grade 316 stainless steel mesh as a counter electrode (CE).
- An aqueous test solution (electrolyte).

Each lid contained two holes: a small center hole for the wire and a second hole for a silver/silver chloride (Ag/AgCl) reference electrode (RE) close to the wire. Figure 6 shows a fully assembled test cell after a test was completed in a 0.4 percent chloride ($[Cl^-]$) solution. A corroded WE and loose corrosion products can be seen inside the cell on the bottom of the cup.

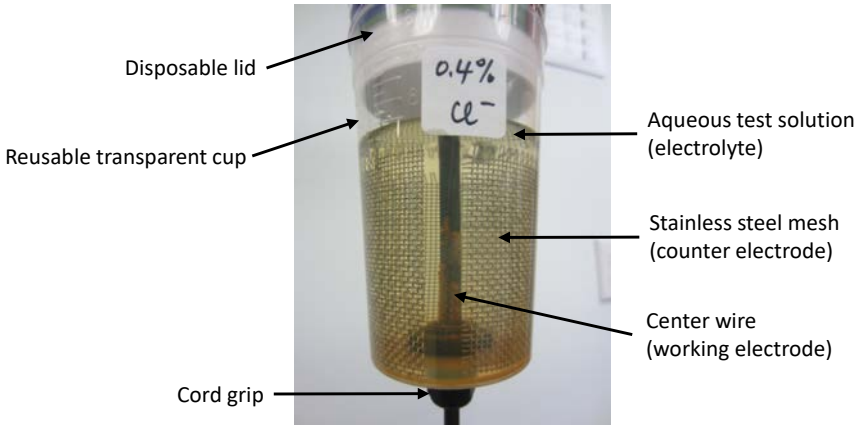

Source: FHWA.

Figure 6. Photo. Test cell mounted on a wire.

As shown in figure 1 through figure 5, multiple test cells were mounted on a single, center wire to test efficiently. Approximately one-third of the test cells were installed on the stressed wires and the others on the unstressed wires. A watertight cord grip attached to the bottom of the plastic cup allowed a single wire to hold multiple test cells without leakage.

After each round of testing, the used test cells were thoroughly cleaned, first with running tap water and then with distilled water, to prevent cross-contamination for the next round of testing with different test solutions.

Electrochemical Test Methods

LPR Measurement

Researchers performed LPR tests for all Batch #1 and Batch #2 specimens to quantify the corrosivity of sulfate ions and compare it against that of chloride ions. Depending on test requirements, either a three-electrode (i.e., WE, CE, and RE) or a two-electrode (i.e., WE and CE/RE) configuration was employed. Figure 7 shows two test cells with different configurations.

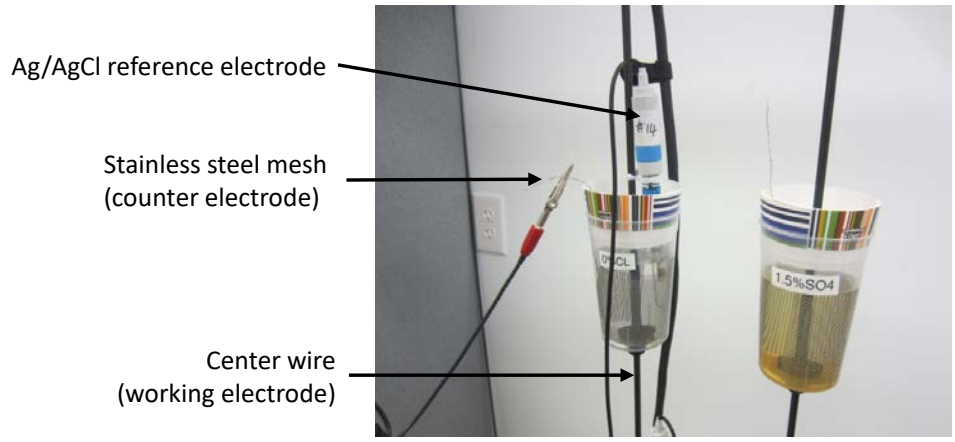

Source: FHWA.

Figure 7. Photo. Three-electrode test cell (left) and two-electrode test cell (right).

For each LPR measurement, a test cell was filled with 5.1 fl oz of a test solution. After approximately 24 h of initial conditioning without disturbances, a potentiostat applied a small increment of direct voltage between the WE and CE, from −15 mV with respect to the specimen's corrosion potential (E_{corr}) to +15 mV, at a scan rate of 0.5 mV/s and a sampling period of 2 s. This process is called polarization. The corresponding current output data in response to each polarized potential step were recorded. Subsequently, the slope of the linear region found between the potential and the current data points, as shown in figure 8, determined the polarization resistance (R) of the specimen by Ohm's law (figure 9).

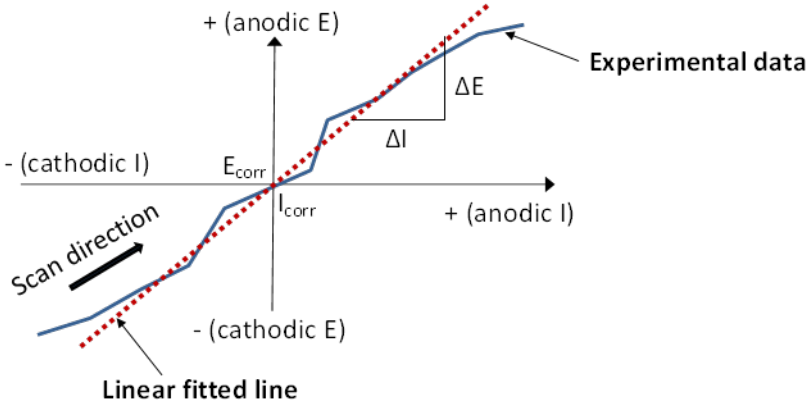

Source: FHWA.

Figure 8. Illustration. LPR measurement.

$$R = E/I$$

Figure 9. Equation. Ohm's law.

A shallower sloped linear region means a lower R and, in turn, a higher corrosion rate. The experimentally determined R was applied to the Stern–Geary equation and Faraday's law to calculate the instantaneous mass loss at the time of measurement in terms of uniform penetration

rate. The most frequently used corrosion rate units are mils per year (mpy) and millimeters per year. In this report, mpy is used.

One problem encountered during this study was that most of the LPR measurements made at the elevated temperature yielded a concave curve instead of a straight line. Figure 10 presents one example of the problem.

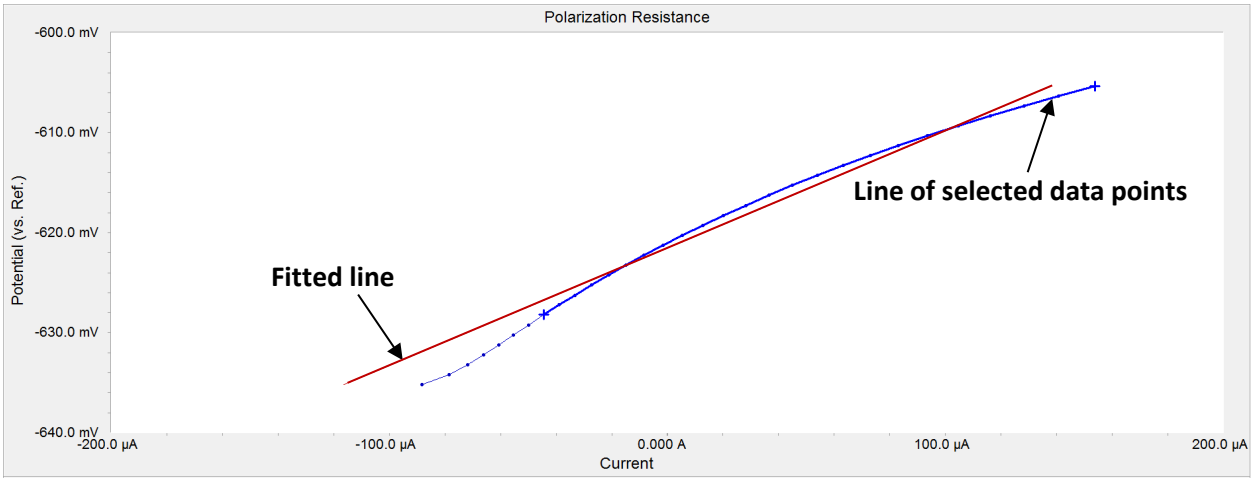

Source: FHWA.

Figure 10. Graph. LPR plot exhibiting continuous corrosion behavior during the measurement.

The concave arc indicated by the curved blue line shows the actual LPR data, while the straight red line represents the theoretical (and expected) linear fit. Researchers reasoned that the specimen corroded continuously, even during the relatively brief measurement duration. To minimize the impact of this problem, the LPR scan range was reduced from ±15 mV to ±10 mV versus corrosion potential, which shortened the measurement time as much as possible.

Corrosion rate calculations used a fixed surface area (SA) of 1.75 inches^2 for Supplier A wires and 1.44 inches^2 for Supplier B wires. These surface areas are based on the immersed wire length in contact with the test solution. A corrosion current (I_{corr}) was converted to corrosion current density (i_{corr}) by dividing by surface area of the specimen. Corrosion current density is an alternative measure to the corrosion rate because the former is linearly proportional to the latter.

CPP Measurement

Researchers used CPP tests to determine the susceptibility of the selected Batch #1 wires to pitting corrosion under different test conditions. Each of the CPP test cells was mounted on a short center wire, and a three-electrode configuration was used. The three lowest sulfate and three lowest chloride concentrations used in Batch #1 were dissolved in four pH solutions, and the CPP tests were performed at the ambient temperature. Each test employed the same anodic polarization scan, starting from about −250 mV versus the specimen's E_{corr}, at a scan rate of 5 mV/s until the polarized potential reached either the apex potential of +1.5 V versus E_{corr} or

apex current density of 10 mA/cm^2. After reaching one of the preset limits, a reverse scan was made toward its original E_{corr} at a scan rate of 2.5 mV/s.

Hypothesis Testing of Corrosion Rate Data

Hypothesis testing is a common statistical technique for understanding the statistical relationship between two data sets. This study tested whether the mean corrosion rates of two data groups should be considered statistically equal or not. Two types of hypothesis tests—the null hypothesis (figure 11) and the alternative hypothesis (figure 12)—were conducted for the sample size of independent group 1 (n_1) and the sample size of independent group 2 (n_2).

$$\mu_1 = \mu_2$$

Figure 11. Equation. Null hypothesis, H_0.

$$\mu_1 > \mu_2$$

Figure 12. Equation. Alternative hypothesis, H_1.

Where:

μ_1 = population mean of independent group 1.
μ_2 = population mean of independent group 2.

Sufficient sample size: When the sum of n_1 and n_2 is greater than 30 data points, reject H_0 and accept H_1 according to the equation in figure 13.

$$Z = \frac{\overline{x} - \overline{y}}{\sqrt{\frac{\sigma_1^2}{n_1} + \frac{\sigma_2^2}{n_2}}} \geq z(\alpha)$$

Figure 13. Equation. Test for hypothesis using normal distribution *Z*.

Where:

$\bar{x}$ = sample mean of data group 1.
$\bar{y}$ = sample mean of data group 2.
σ_1 = population variance of independent group 1.
σ_2 = population variance of independent group 2.
$z(\alpha)$ = normal distribution probability with a significance level $\alpha = 0.025$.

Insufficient sample size: When the sum of n_1 and n_2 is less than or equal to 30 data points, using the equation in figure 14, reject H_0 and accept H_1.

$$T = \frac{\overline{x} - \overline{y}}{\sqrt{\frac{(n_1 - 1)s_x^2 - (n_2 - 1)s_y^2}{n_1 + n_2 - 2}\left(\frac{1}{n_1} + \frac{1}{n_2}\right)}} \geq t(\alpha;\ n_1 + n_2 - 2)$$

Figure 14. Equation. Test for hypothesis using Student's *t*-Distribution *T*.

Where:

s_x^2 = sample variance of data group 1.

s_y^2 = sample variance of data group 2.

$t(\alpha)$ = Student's *t*-distribution probability with a significance level $\alpha = 0.025$.

Several pairs of mean corrosion rate data were compared according to the following variables:

- Sulfate ions versus chloride ions.
- Stressed wires versus unstressed wires.
- Wires in as-received surface condition versus cleaned surface condition.
- Supplier A strands versus Supplier B strands.

When one pair of the variables was tested, all the relevant corrosion rate data were grouped according to the two variables. For example, when the variable pair stressed wires versus unstressed wires was tested, all corrosion rate data generated under different temperatures (77 and 104 °F), anion types (sulfate and chloride), and pH (8.0, 10.0, 12.5, and 13.6) were regrouped only by stress conditions.

TASK 2: CHARACTERIZATION OF GROUT SAMPLES

Raw Grout Samples

Researchers examined the characteristics of raw grout samples from three products in terms of bag weight and chemical composition analysis. Each grout bag was weighed individually at the beginning of this task, and the results are summarized in table 4.

Table 4. Grout bag weights.

Grout Product	Number of Bags Measured	Nominal Weight (lb)	Mean (lb)	Median (lb)	SDEV (lb)	Max (lb)	Min (lb)
Product 1	20	50.0	51.5	50.5	1.7	54.5	49.5
Product 2	20	55.0	55.2	55.4	0.4	56.0	54.0
Product 3	3	50.0	52.2	52.5	0.6	52.5	51.5

SDEV = standard deviation; Max = maximum; Min = minimum.

According to the weight measurement results, Product 1 bags exhibited the most significant variation among the three products, with a standard deviation (SDEV) of 1.7 lb or a coefficient of variation of 3.3 percent. The others showed little variation, although Product 3 data could not be statistically significant due to an insufficient number of leftover bags. It is recommended that specifications express the upper and lower limits on bag weight variation in percentages.

Thirteen representative raw grout samples were collected from each of the selected bags for chemical composition analysis. For grout sampling of Product 1 and Product 2, the lightest, heaviest, and median weight bags within each group were selected. For Product 3, all remaining bags were used.

During the grout handling and documentation process, the grout expiration date could not be identified easily for Product 1 and Product 2. Their bags were stamped with unique codes that

cannot be understood by ordinary end users. In contrast, Product 3 clearly showed "manufactured on" and "use by" dates. Since grout expiration date is a critical piece of information for quality control in the field, this report recommends a unified package labeling system that identifies expiration dates for all prepackaged grout products.

Hardened Grout Specimens

For each product, three 4- by 8-inch cylindrical specimens were fabricated in three batches. Each batch used 20 lb of grout randomly taken from three different bags and mixed with the following maximum water dosages recommended by the manufacturers:

- Product 1: 5.7 lb (14.2 lb recommended for a 50-lb bag).
- Product 2: 6.4 lb (17.5 lb recommended for a 55-lb bag).
- Product 3: 5.0 lb (12.5 lb recommended for a 50-lb bag).

A fourth cylindrical specimen of each product was also made by adding 0.5 lb of water to the leftover mix after the three cylindrical specimens were cast. Researchers used these fourth specimens to investigate grout segregation tendency in the presence of a modest amount of extra water. All specimens were cured for 7 days at room temperature.

Once the specimens were cured and demolded, a grout sample was scraped off the top of each specimen and analyzed for free sulfate ions in the top layer. Figure 15 shows the top surface of a cylindrical specimen that has been scraped mechanically with a chisel and the collected grout sample.

Source: FHWA.

Figure 15. Photo. Grout sample scraped from the top layer of a cylindrical specimen of Product 3.

Following the top layer grout sampling, three 1.0-inch-thick slices were cut from each cylindrical specimen at three different depths—top, mid-depth, and bottom—using a wet masonry saw. Then each slice was cut in half. For each slice, one half was pulverized for free sulfate analysis (54 powder samples), and the other half was stored for future petrographic analysis.

Petrographic Examination and Chemical Analyses

Once the necessary grout samples were prepared in the laboratory, three hardened grout samples made of #1 Old Product 3 and a raw grout powder sample from #2 Old Product 3 were sent to an independent laboratory for petrographic analysis, in accordance with the pertinent sections of *ASTM C856: Standard Practice for Petrographic Examination of Hardened Concrete*, and chemical analyses applicable to grout materials.[15] In addition, one field grout sample containing soft and hard portions retrieved from the Ringling Causeway Bridge in Florida was included for comparison against the laboratory prepared samples. Table 5 contains detailed information about these samples.

Table 5. Sample information for petrographic examination and chemical analyses.

Sample ID	Sample Description	Mixing Water	Grout Material
#1 P3-2M	Hardened grout from the middle section of a 4- by 8-inch cylindrical specimen	5.0 lb per manufacturer's recommendation	#1 Old Product 3 acquired in 2009
#1 P3-2B	Hardened grout from the bottom section of a 4- by 8-inch cylindrical specimen	5.0 lb per manufacturer's recommendation	#1 Old Product 3 acquired in 2009
#1 P3-4 xtra T	Hardened grout from the top section of a 4- by 8-inch cylindrical specimen with higher water content	Additional 0.5 lb of water was added to leftover mix to create segregated grout	#1 Old Product 3 acquired in 2009
Raw material	Raw grout powder	Not applicable	#2 Old Product 3 acquired in 2012
403-6L (soft)	Field sample of segregated (soft) grout extracted from a high point of an external tendon	Unknown	Product 3
403-6L (hardened)	Field sample of segregated (hardened) grout extracted from a high point of an external tendon	Unknown	Product 3

ID = identifier; M = middle; B = bottom.

To characterize the grout samples, researchers employed stereomicroscopy, comparative thin-section microscopy, X-ray diffraction (XRD), and chemical analyses for total sulfur content and water-soluble sulfate content (*ASTM C1580*: *Standard Test Method for Water-Soluble Sulfate in Soil*, modified for cementitious materials).[18] The crystalline components in the grout samples were determined with XRD. The total sulfur content, which was reported as percent sulfur trioxide (SO_3) by mass of sample, was determined using evolution and infrared detection.

TASK 3: DETERMINATION OF WATER-SOLUBLE SULFATE IONS IN THE RAW GROUT POWDERS AND HARDENED GROUT SPECIMENS

To determine the total amounts of free sulfate ions in the raw grout powders and hardened grout specimens, researchers used ion chromatography (IC). In most cases, approximately 0.018 oz of each grout powder sample was dissolved in 16.9 fl oz of deionized water for 24-h leaching before IC analysis.

CHAPTER 4. TEST RESULTS AND DISCUSSION

STRAND CONDITION

The strand material acquired from Supplier A was covered with a drawing lubricant. Information about the lubricant was not available from the strand supplier. No sign of corrosion was observed on the exterior wire surface with the naked eye. However, corrosion products were discovered on the center wire surface, even in the presence of the lubricant. The representative condition of a center wire is shown in figure 16.

Source: FHWA.

Figure 16. Photo. Close-up view of a center wire extracted from a Supplier A strand.

The corrosion products disappeared easily after rubbing the wire surface with a paper towel. Since the observed corrosion products were superficial, suggesting no permanent corrosion damage to the wires, it was suspected that the strands were briefly exposed to moisture. Thus, the as-received center wires not exhibiting corrosion damage were used for Batch #1, except for some wires that were cleaned. The diameter of the center wires was 0.209 inches.

The supplementary strand material acquired from Supplier B did not appear to have a drawing lubricant, and some outer wire sections had sustained heavy rust. However, the extracted center wires did not exhibit rust, even though they had little lubricant on the surface. The representative condition of a center wire is shown in figure 17.

Source: FHWA.

Figure 17. Photo. Close-up view of a center wire extracted from a Supplier B strand.

Like Supplier A's wires, the as-received center wires from supplier B were used for Batch #1, except for some wires that were cleaned. The diameter of Supplier B's center wires was 0.170 inches.

The additional strand material acquired from Supplier C was also covered with a drawing lubricant. No sign of corrosion was observed on the wire surface with the naked eye. The representative condition of a center wire is shown in figure 18.

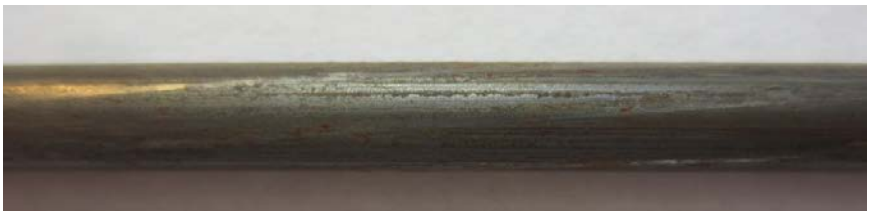

Source: FHWA.

Figure 18. Photo. Close-up view of a center wire extracted from a Supplier C strand.

The as-received center wires from supplier C were used for Batch #2. The diameter of Supplier C's center wires was 0.200 inches.

OVERVIEW OF LPR DATA

The collected LPR data exhibited a wide range of corrosion rates depending on the experimental conditions. In general, a shallower sloped linear region, accompanied by widely spaced potential-current data points, suggested a lower polarization resistance and higher corrosion rate. As expected, anion-free solutions yielded the lowest corrosion rate at any pH. In test solutions containing a particular ionic concentration, the wires tested at the elevated temperature and in low-pH solutions experienced higher corrosion rates (i.e., lower polarization resistances) than those exposed to ambient temperature and high pH. They also exhibited a higher corrosion tendency by showing more negative potential. For example, the LPR plots of two wires exposed to anion-free pH 8.0 solutions at ambient temperature exhibited steeper and shorter linear regions than two other wires exposed to 0.4 percent sulfate and 0.4 percent chloride solutions at the same pH and temperature. The corresponding corrosion rate of the anion-free wires was 0.050 mpy, which is much less than those of the wires exposed to 0.4 percent sulfate (6.1 mpy) and 0.4 percent chloride (5.2 mpy). At the elevated temperature, the calculated corrosion rates increased to 0.61 (anion-free), 9.0 (sulfate), and 9.6 (chloride) mpy, respectively.

The LPR data also indicated that similar concentrations of sulfate and chloride ions behaved similarly in lower pH environments (8.0 and 10.0). However, in higher pH environments (12.5 and 13.6), sulfate became less aggressive than chloride, regardless of temperature.

OVERVIEW OF CPP DATA

Figure 19 through figure 26 present data from the CPP tests of unstressed wires collected at ambient temperature in four pH solutions (8.0, 10.0, 12.5, and 13.6). Each figure shows three CPP plots of data obtained from either three sulfate solutions ($[SO_4^{2-}]$ = 0.2, 0.4, and 0.8 percent) or three chloride solutions ($[Cl^-]$ = 0.08, 0.4, and 0.8 percent) at a given pH.

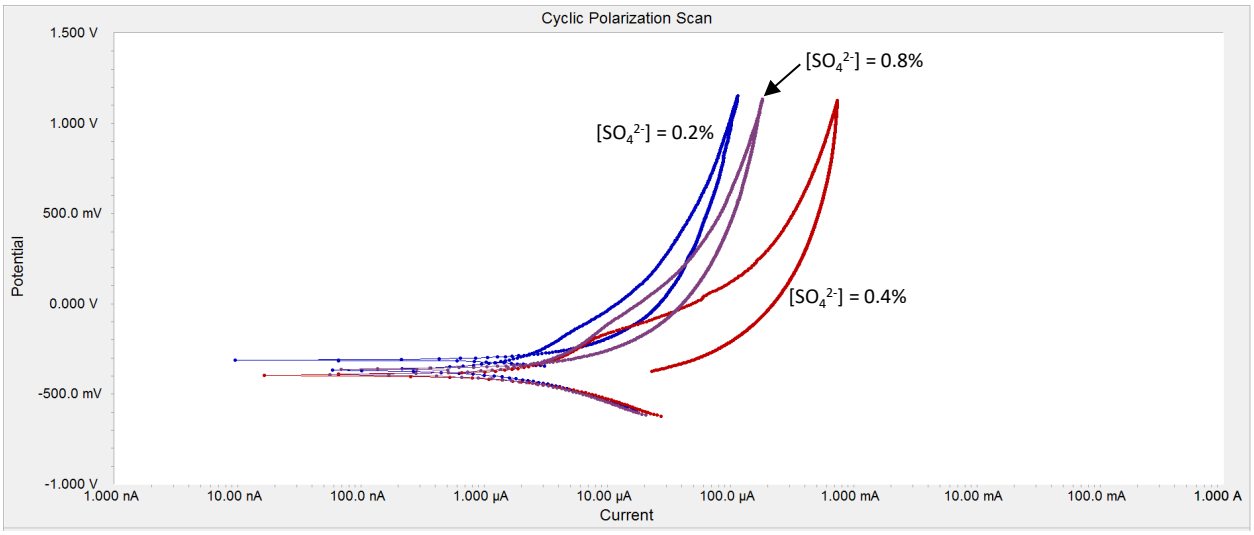

Source: FHWA.
25 °C = 77 °F.

Figure 19. Graph. CPP data from unstressed wires exposed to three [SO_4^{2-}] in pH 8.0 solutions.

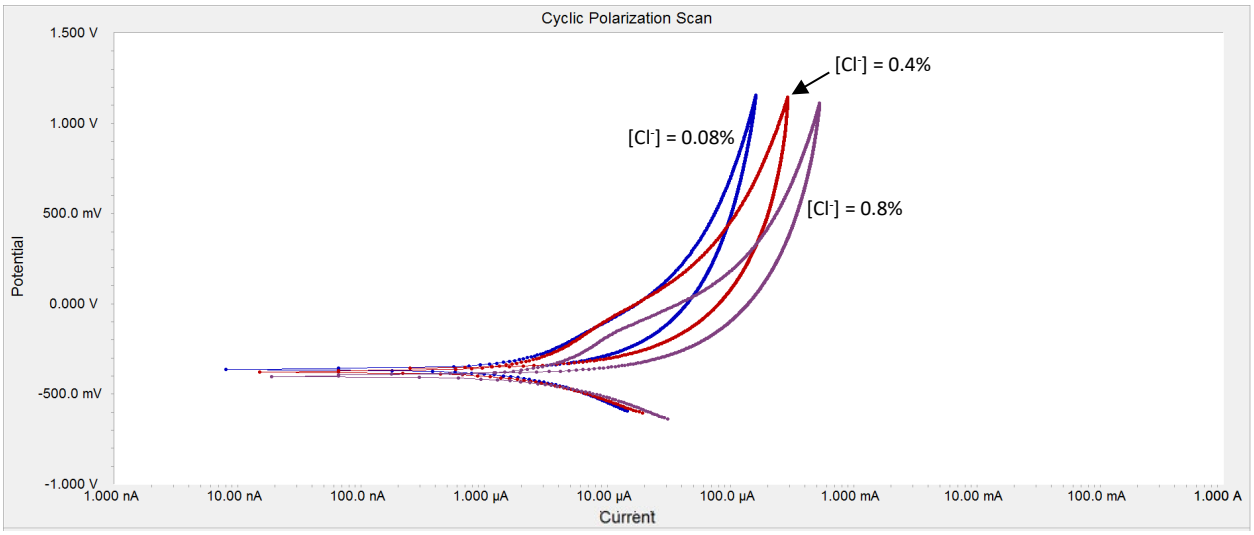

Source: FHWA.
25 °C = 77 °F.

Figure 20. Graph. CPP data from unstressed wires exposed to three [Cl^-] in pH 8.0 solutions.

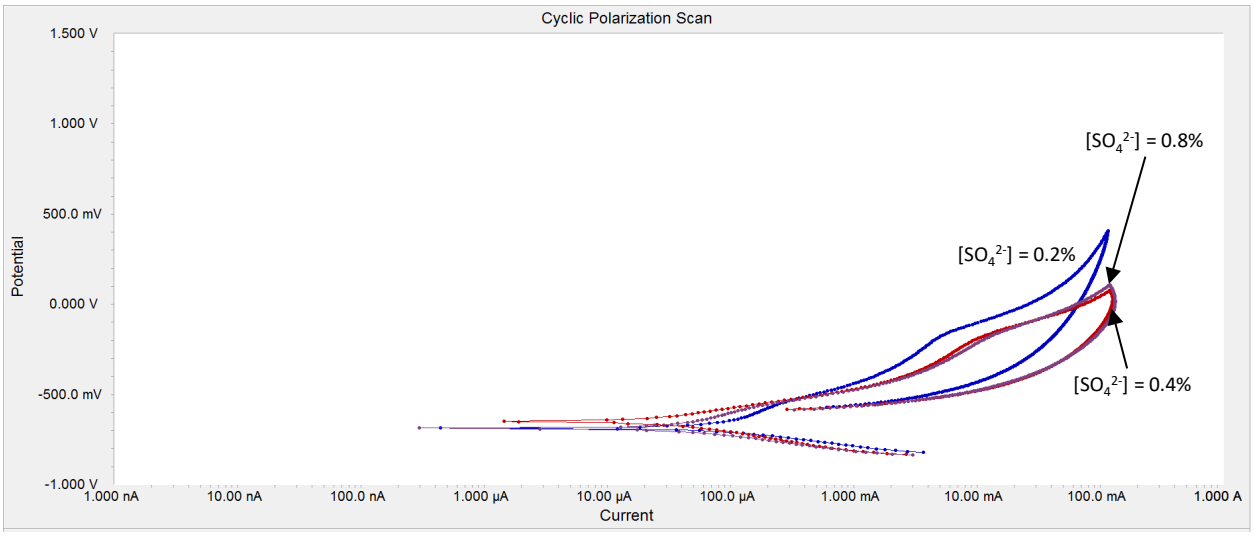

Source: FHWA.
25 °C = 77 °F.

Figure 21. Graph. CPP data from unstressed wires exposed to three [SO_4^{2-}] in pH 10.0 solutions.

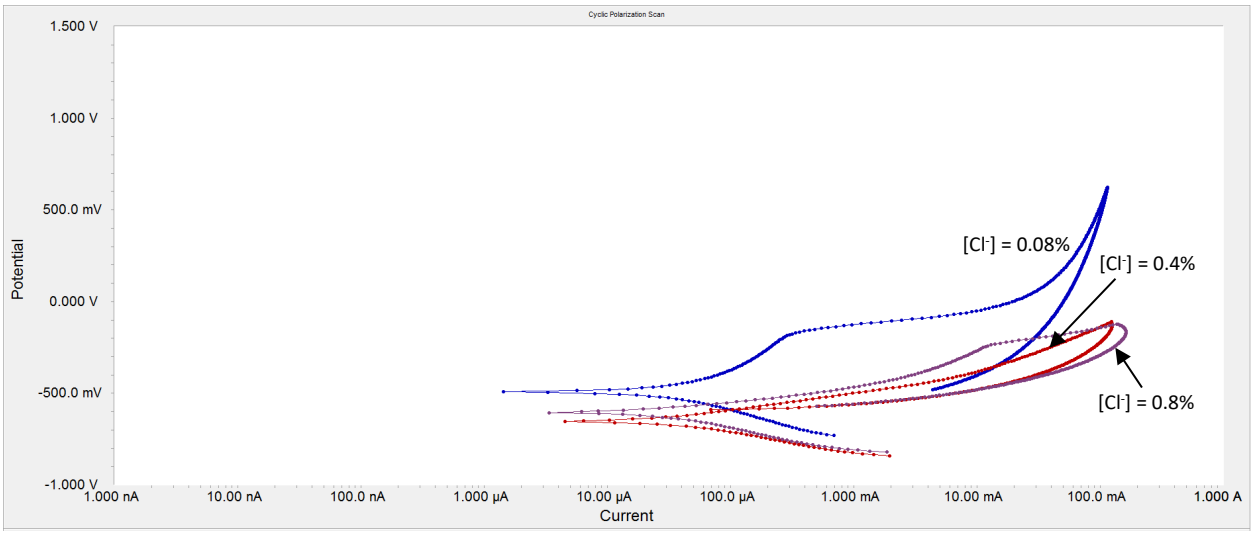

Source: FHWA.
25 °C = 77 °F.

Figure 22. Graph. CPP data from unstressed wires exposed to three [Cl^-] in pH 10.0 solutions.

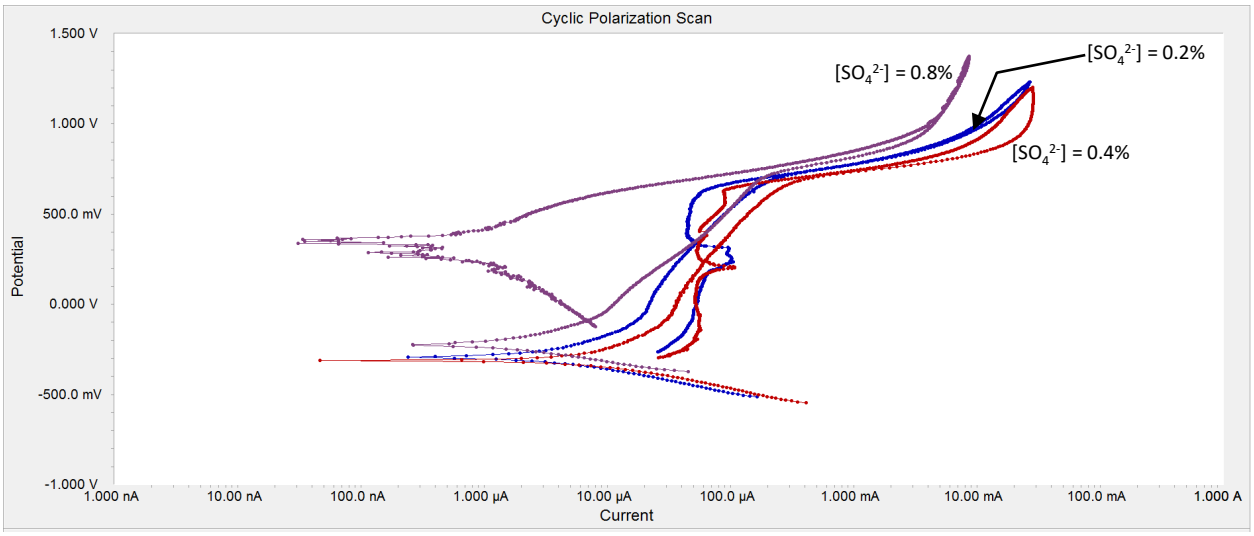

Source: FHWA.
25 °C = 77 °F.

Figure 23. Graph. CPP data from unstressed wires exposed to three [SO_4^{2-}] in pH 12.5 solutions.

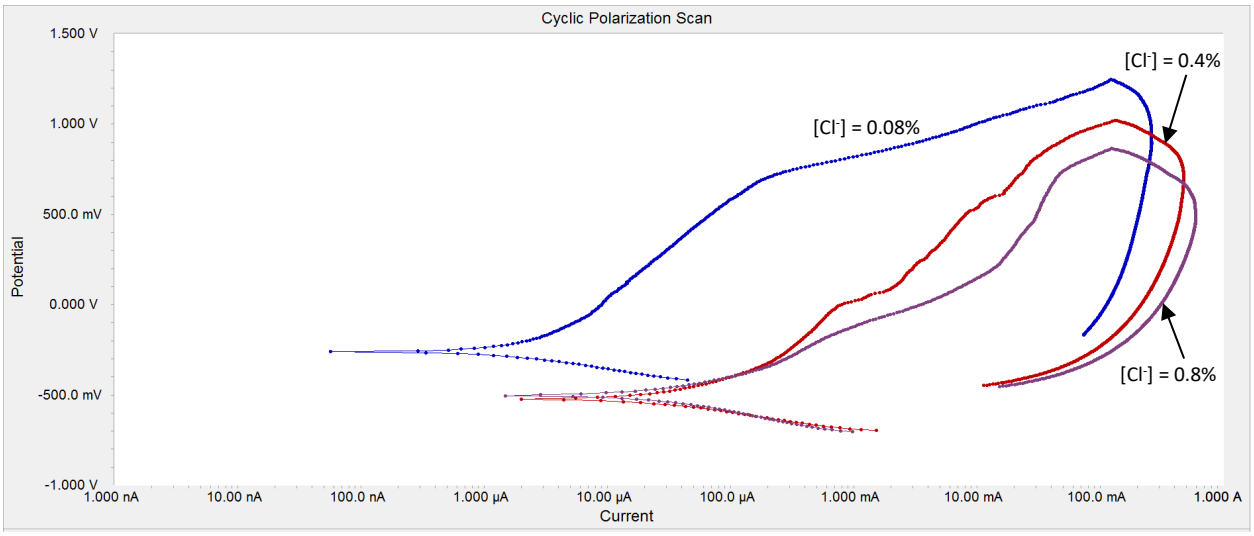

Source: FHWA.
25 °C = 77 °F.

Figure 24. Graph. CPP data from unstressed wires exposed to three [Cl^-] in pH 12.5 solutions.

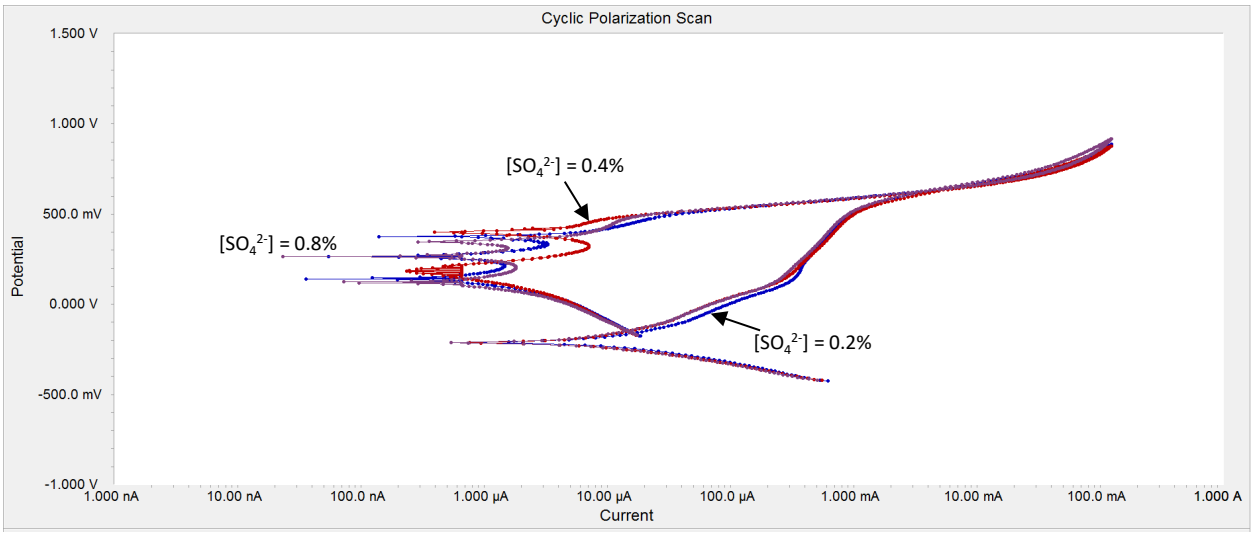

Source: FHWA.
25 °C = 77 °F.

Figure 25. Graph. CPP data from unstressed wires exposed to three [SO_4^{2-}] in pH 13.6 solutions.

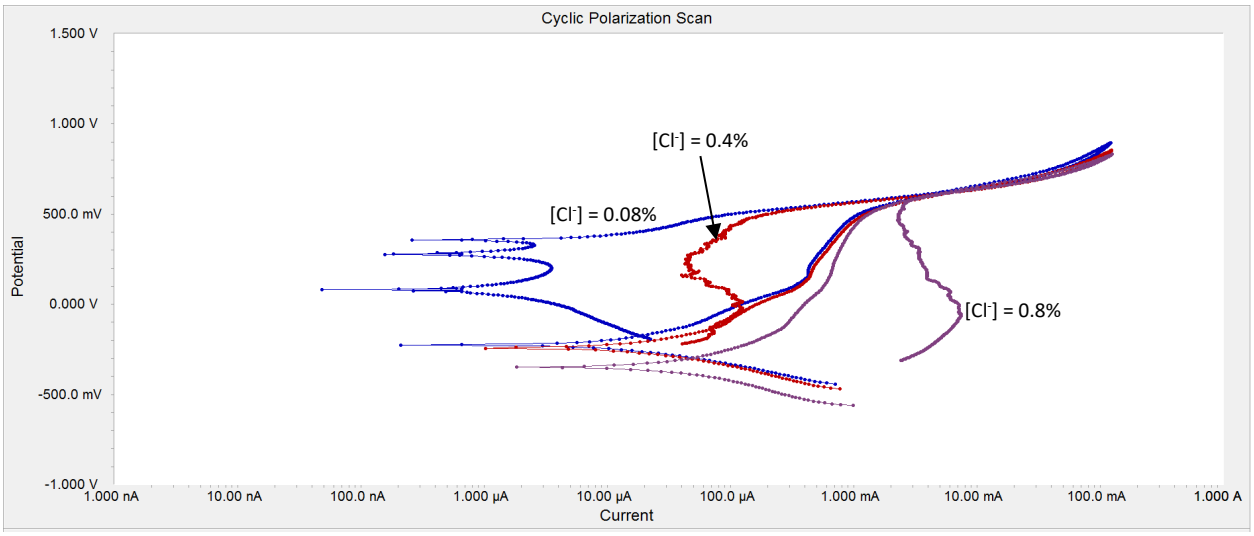

Source: FHWA.
25 °C = 77 °F.

Figure 26. Graph. CPP data from unstressed wires exposed to three [Cl^-] in pH 13.6 solutions.

The wires exposed to sulfate and chloride ions in the pH 8.0 and 10.0 solutions showed similar CPP behaviors of pitting corrosion: no passivity (pH 8.0 in figure 29 and figure 30) and very weak passivity (pH 10.0 in figure 21 and figure 22). The wires tested in the pH 12.5 and 13.6 sulfate solutions exhibited pitting resistant behavior, as presented in figure 23 and figure 25, respectively. The wires tested in the pH 12.5 chloride solutions did not show good pitting resistance (figure 24); however, good pitting resistance appeared in the pH 13.6 chloride solutions (figure 26). Thus, chloride ions appeared more aggressive than sulfate ions in an alkaline environment. In all cases, pH was a more influential parameter than ionic concentration

in determining pitting resistance. These results suggest that pH is the critical factor in determining the pitting resistance of metals and alloys.

ANALYSES OF CORROSION RATE AND CORROSION POTENTIAL DATA

Instantaneous Corrosion Rate

Instantaneous corrosion rate indicates the kinetic aspect of corrosion and quantifies how fast corrosion can take place at the time of the measurement. This quantity is critical information to determine corrosion intensity in a given environment.

Figure 27 and figure 28 show mean corrosion rates of Batch #1 and Batch #2 versus pH plots for the wires exposed to eight sulfate concentrations and one sulfate-free solution at 77 and 104 °F, respectively. Each legend entry indicates nominal pH, actual pH, and batch number (Batch #1 designated as 1st and Batch #2 as 2nd).

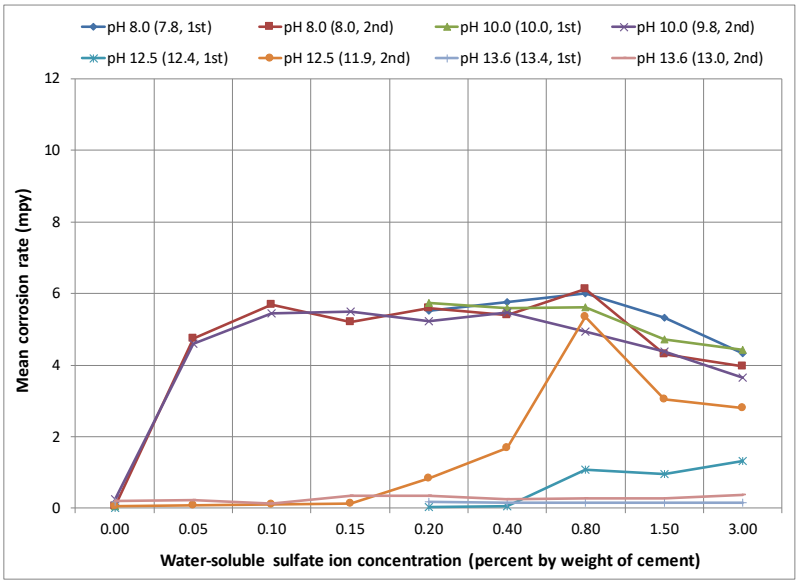

Source: FHWA.

Figure 27. Graph. Mean corrosion rate data from Batch #1 and Batch #2 in [SO_4^{2-}] solutions at 77 °F.

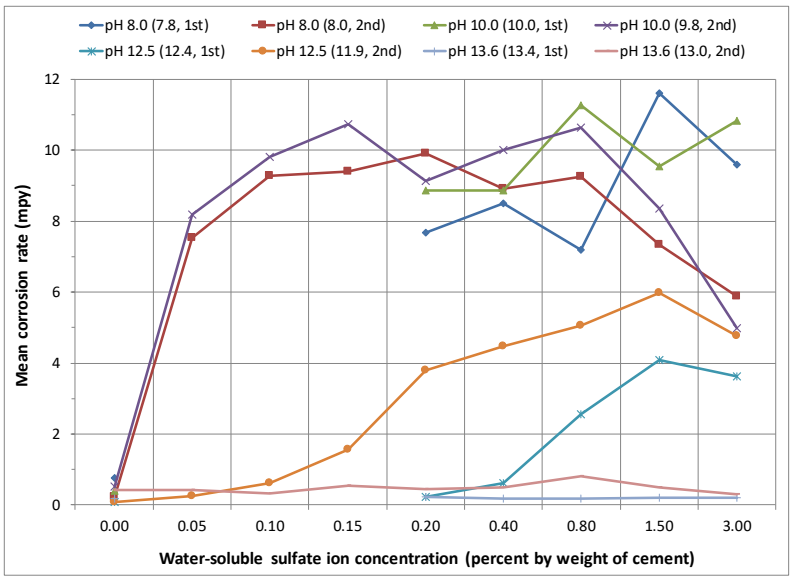

Source: FHWA.

Figure 28. Graph. Mean corrosion rate data from Batch #1 and Batch #2 in [SO_4^{2-}] solutions at 104 °F.

Anion-free solutions yielded virtually zero corrosion rates, regardless of pH and temperature. Sulfate-induced corrosion was also negligible in the high-pH solutions (actual pH > 13.0), irrespective of sulfate concentration and temperature. Under the other test conditions, sulfate concentration, pH, and temperature influenced the mean corrosion rate. When 0.05 percent sulfate ions were added to the sulfate-free pH 8.0 (actual pH 7.8 and 8.0) and pH 10.0 (actual pH 9.8 and 10.0) solutions, the corrosion rate jumped more than four times at 77 °F and seven times at 104 °F, followed by a small, gradual increase in the corrosion rate up to 0.8 percent sulfate. With further increased sulfate concentration in these pH solutions, corrosion rates gradually decreased, probably due to the release of initially dissolved oxygen in the solution in the presence of excessive anions. The mean corrosion rate data collected at 77 °F showed this trend clearly. When the temperature was increased to 104 °F, the mean corrosion rates nearly doubled, despite some data fluctuation. These trends suggest that the sulfate threshold for corrosion initiation may be as low as 0.05 percent in lower pH (i.e., carbonated) environments, and that temperature influences the corrosion rate more than the sulfate concentration up to 0.8 percent.

In an intermediate pH of 12.5 (actual pH 11.9 and 12.4), the mean corrosion rate was substantially reduced compared to those obtained in the lower pH solutions. The actual pH 11.9 solution yielded higher mean corrosion rates than the pH 12.4 solution. The former (pH 11.9 solution) increased the corrosion rate steadily when sulfate concentration increased from 0.2 to 0.8 percent at 77 °F, and from 0.15 to 1.5 percent at 104 °F. In contrast, the latter (pH 12.4 solution) further reduced corrosion rates at every sulfate concentration. As the actual pH increased from 11.9 to 12.4, and ultimately to 13.4, the corrosion rate dropped noticeably.

Figure 29 and figure 30 show mean corrosion rates for five Batch #1 chloride concentrations in four different pH solutions at 77 and 104 °F, respectively.

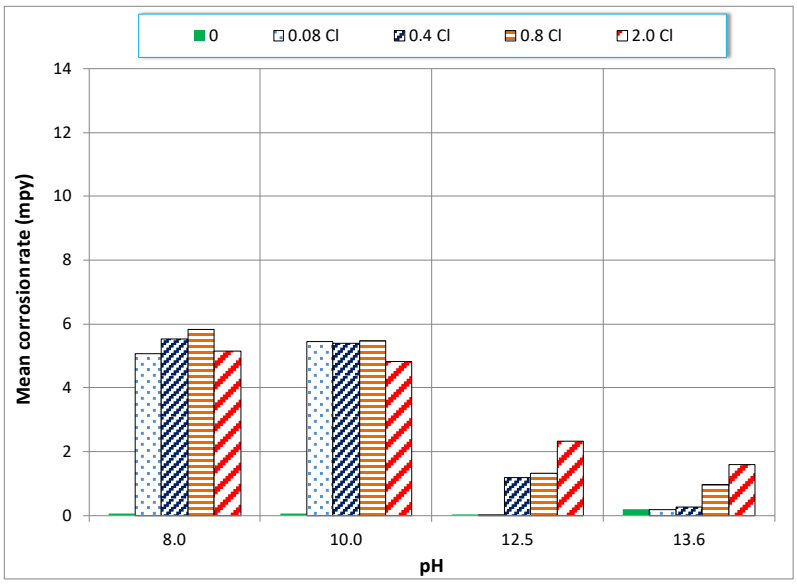

Source: FHWA.

Figure 29. Graph. Mean corrosion rate data from Batch #1 in [Cl^-] solutions at 77 °F.

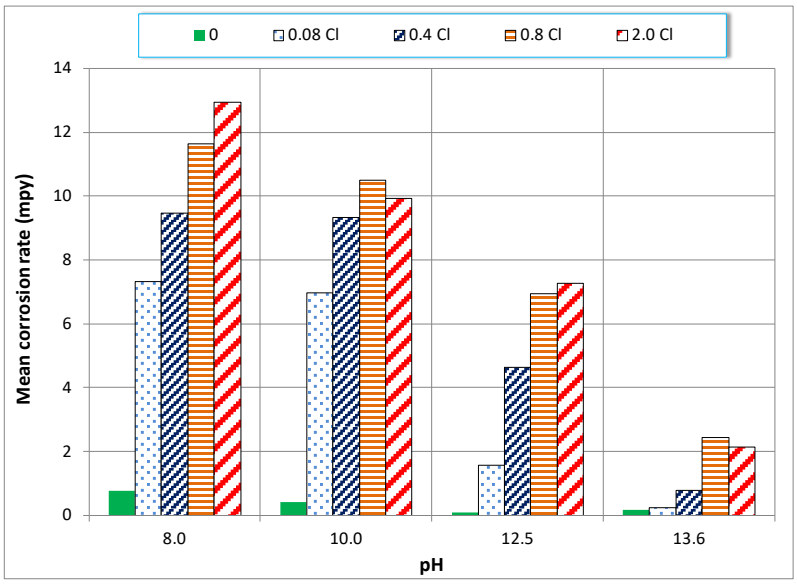

Source: FHWA.

Figure 30. Graph. Mean corrosion rate data from Batch #1 in [Cl^-] solutions at 104 °F.

Sulfate and chloride produced comparable mean corrosion rates in the two lower pH solutions at the ambient and elevated temperatures. However, in higher pH environments, chloride became more aggressive than sulfate at both temperatures, meaning chloride induced higher mean corrosion rates than sulfate did. The aggressiveness of chloride ions is particularly noticeable in pH 12.5 at 104 °F. To compare the corrosion rate data statistically, hypothesis testing was performed, and its results are summarized in table 6.

Table 6. Hypothesis testing of mean corrosion rates in sulfate versus chloride solutions.

Category	pH 8.0		pH 10.0		pH 12.5		pH 13.6	
Anion type	Cl^-	SO_4^{2-}	Cl^-	SO_4^{2-}	Cl^-	SO_4^{2-}	Cl^-	SO_4^{2-}
Number of samples	67	54	58	47	56	47	76	55
Sample mean	5.812	6.244	6.747	7.571	3.069	1.582	0.765	0.183
Sample variance	18.021	11.406	11.947	6.299	6.218	2.190	0.656	0.014
Sample SDEV	4.245	3.377	3.456	2.510	2.494	1.480	0.810	0.117
Median	6.158	6.172	6.458	6.759	2.416	1.258	0.250	0.179
Z	−0.623		−1.413		3.745*		6.173*	
$z(\alpha = 0.025)$	1.965							

*Accepts alternative hypothesis, H_1.

The testing results accept H_0 (null hypothesis; μ_1 (chloride) = μ_2 (sulfate)) in the pH 8.0 and 10.0 solutions and accept H_1 (alternative hypothesis; μ_1 (chloride) > μ_2 (sulfate)) in the pH 12.5 and 13.6 solutions. In other words, sulfate is a weaker species than chloride in higher pH solutions. This conclusion also confirms the observation, made with the CPP data presented in figure 33 and figure 34, that chloride ions are still aggressive at pH 12.5; in contrast, the wires in sulfate solutions at the same pH exhibited some pitting resistance.

Figure 31 presents the mean corrosion rate data from Batch #1 measured at 32 °F in pH 8.0 and 13.6 solutions that contained three concentrations (0, 0.4, and 0.8 percent) of sulfate and chloride ions.

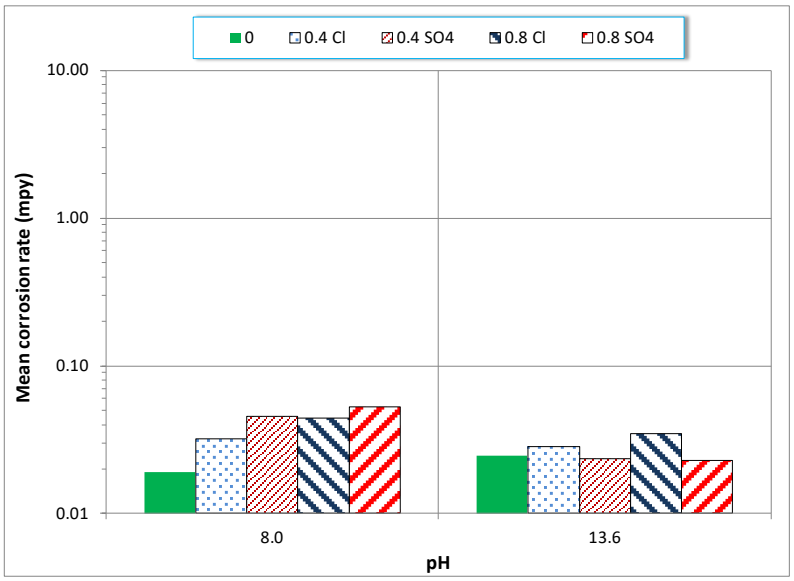

Source: FHWA.

Figure 31. Graph. Mean corrosion rate data from Batch #1 at 32 °F.

A near-freezing temperature suppressed corrosion in every condition and yielded negligible mean corrosion rates. A logarithmic scale plot was used to highlight the drastically reduced corrosion rates.

The effect of stress on the corrosion rate was also examined after regrouping Batch #1 data by unstressed versus stressed conditions. Figure 32 shows a scatter plot of mean corrosion rates for unstressed and stressed wires immersed in sulfate and chloride solutions.

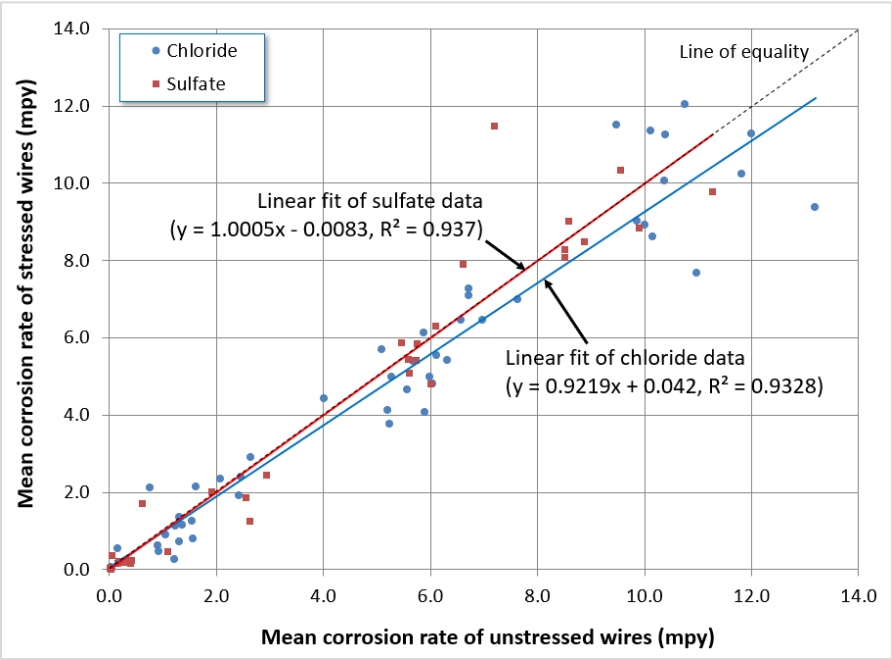

Source: FHWA.

Figure 32. Graph. Mean corrosion rate data from Batch #1 unstressed versus stressed wires in [Cl^-] and [SO_4^{2-}] solutions.

The linear fit of the sulfate data fell precisely on the line of equality with a coefficient of determination (R^2) of 0.937, indicating that there was virtually no difference between the unstressed and stressed data groups. The linear fit of the chloride data deviated slightly from the line of equality, but an R^2 of 0.933 and slope of nearly one suggested that stress had a negligible effect on the corrosion rate in chloride solutions as well. The hypothesis testing results also confirmed that the mean corrosion rates of the unstressed wires were statistically equal to those of the stressed wires in every pH environment tested.

Figure 33 shows that chloride was more aggressive than sulfate when equal concentrations (0.4 or 0.8 percent) of sulfate and chloride ions were mixed in the test solutions. Also, mean corrosion rates were similar to those for the same chloride concentrations without sulfate ions. As expected, the elevated temperature yielded higher corrosion rates than the ambient temperature.

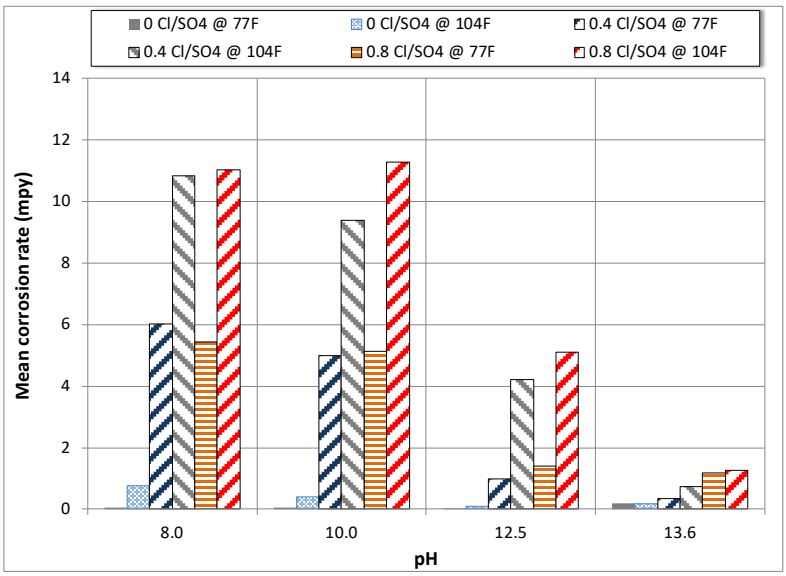

Source: FHWA.

Figure 33. Graph. Mean corrosion rate data from Batch #1 in $[Cl^-]+[SO_4^{2-}]$ solutions.

After Batch #1 mean corrosion rate data were regrouped by uncleaned wires versus cleaned wires, hypothesis testing was performed to investigate the effect of surface cleaning on corrosion. The results verify that the mean corrosion rates of the uncleaned wires were statistically equal to those of the cleaned wires under all tested conditions.

Similar hypothesis testing was performed using the mean corrosion rates of Supplier A and Supplier B wires. Both products were tested without tension and exposed to 0.4 and 0.8 percent of sulfate and chloride ions dissolved in four pH solutions. The hypothesis testing results indicated that the mean corrosion rates of the Supplier A wires were statistically equal to those of the Supplier B wires in the pH 8.0 and 10.0 solutions. However, the Supplier A wires exhibited higher corrosion rates than the Supplier B wires in the pH 12.5 sulfate solutions and pH 13.6 chloride solutions. It is unclear what caused higher corrosion rates in the Supplier A wires under those conditions.

Corrosion Potential

Corrosion potential indicates the thermodynamic aspect of the corrosion process (i.e., whether corrosion can take place thermodynamically or not). It is critical information to assess the likelihood of corrosion in a given environment. A more negative potential with respect to an RE is more likely to initiate corrosion. By analyzing corrosion rate data and corrosion potential data together, the corrosion risk of a specific exposure condition (or site) can be fully understood.

Figure 34 and figure 35 show mean corrosion potential data from Batch #1 and Batch #2 exposed to eight sulfate concentrations in eight pH solutions at 77 and 104 °F, respectively. Figure 36 and figure 37 show the same type of data in five chloride concentrations.

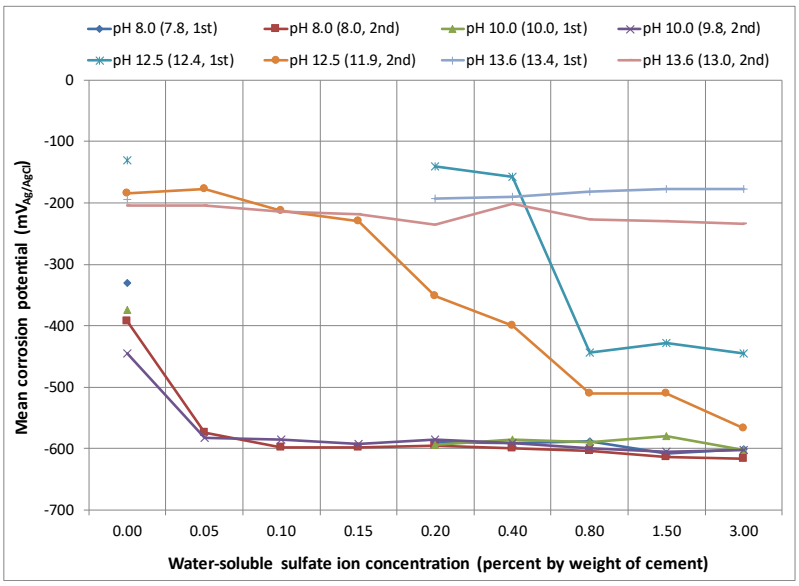

Source: FHWA.

Figure 34. Graph. Mean corrosion potential data from Batch #1 and Batch #2 in [SO_4^{2-}] solutions at 77 °F.

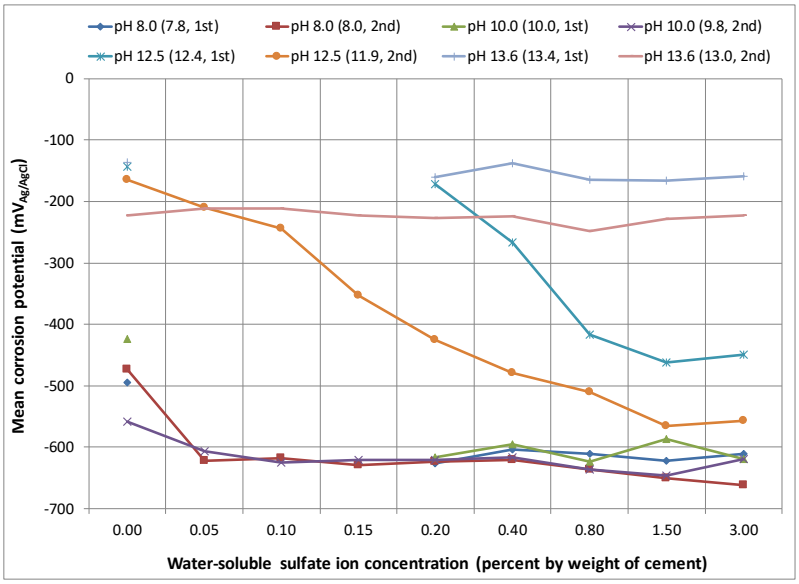

Source: FHWA.

Figure 35. Graph. Mean corrosion potential data from Batch #1 and Batch #2 in [SO_4^{2-}] solutions at 104 °F.

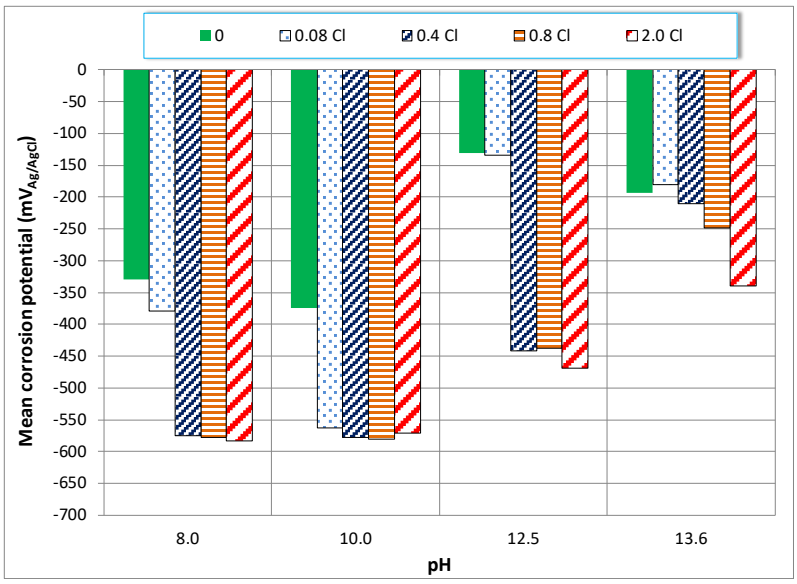

Source: FHWA.

Figure 36. Graph. Mean corrosion potential data from Batch #1 in [Cl⁻] solutions at 77 °F.

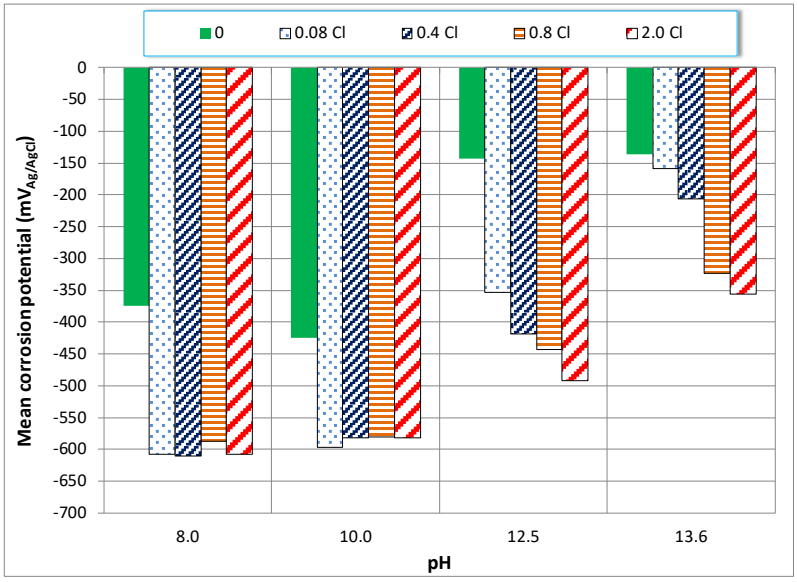

Source: FHWA.

Figure 37. Graph. Mean corrosion potential data from Batch #1 in [Cl⁻] solutions at 104 °F.

As observed in the mean corrosion rate data, anion-free solutions were the least aggressive, as evidenced by the most positive mean corrosion potentials at each pH. In the other solutions containing various amounts of anions, the higher pH solutions (12.5 and 13.6) produced more positive mean corrosion potentials than the lower pH solutions. In particular, sulfate was more sensitive to a pH change than chloride. The mean corrosion potentials measured in the lower pH solutions (8.0 and 10.0) containing sulfate and chloride ions showed a more active corrosion tendency (more negative potential). The mean corrosion potentials did not change much when ionic concentrations increased.

Corrosion Rate versus Corrosion Potential Relationship

Figure 38 shows the relationship between individual corrosion rate data and the corresponding corrosion potential data, grouped by anion type and temperature in pH 8.0 solutions.

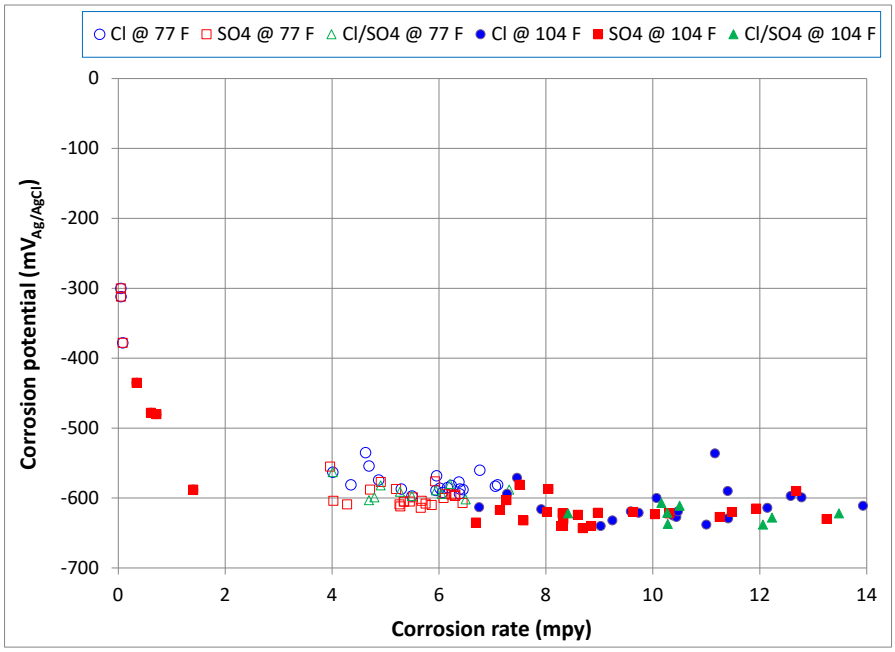

Source: FHWA.

Figure 38. Graph. Relationship between mean corrosion rate and mean corrosion potential data from Batch #1 in pH 8.0 solutions.

Due to the lack of passivity, all the potential data in the chloride solutions and in most of the sulfate solutions were in the active potential region, near −600 mV versus Ag/AgCl RE ($mV_{Ag/AgCl}$), and the corresponding corrosion rates exceeded 4 mpy.

A similar plot for the pH 13.6 data is presented in figure 39.

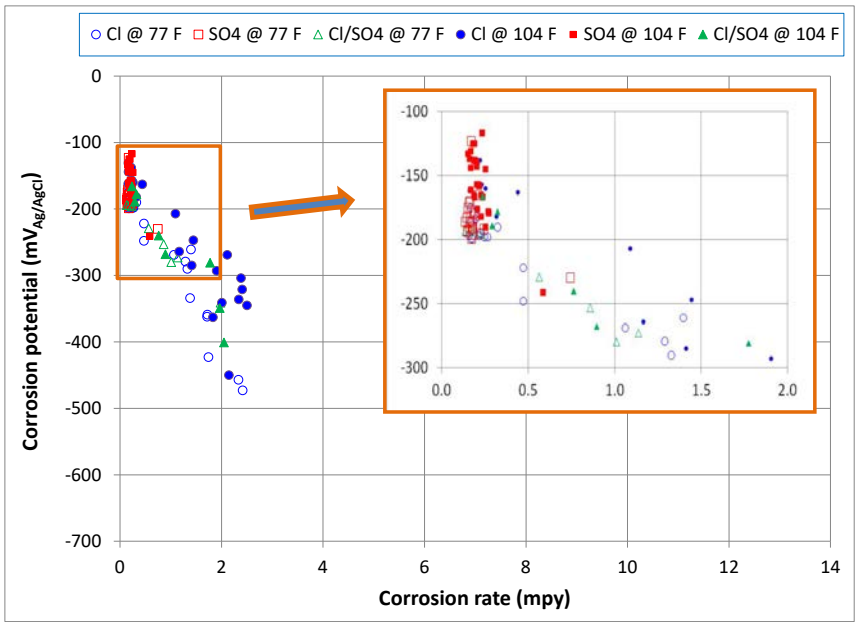

Source: FHWA.

Figure 39. Graph. Relationship between corrosion rate and corrosion potential data from Batch #1 in pH 13.6 solutions.

Unlike the trend presented in figure 38 for pH 8.0 solutions, corrosion potentials for pH 13.6 were relatively positive, and most of the corresponding corrosion rates were less than 2 mpy because of passivity maintained in the highly alkaline environment. The inset shows that sulfate was noticeably less corrosive than chloride, as shown by a potential more positive than −200 $mV_{Ag/AgCl}$ and corrosion rate lower than 0.3 mpy.

Figure 40 shows the relationship between individual corrosion rate data from Batch #2 and the corresponding corrosion potential data, grouped by the actual pH and all sulfate concentrations.

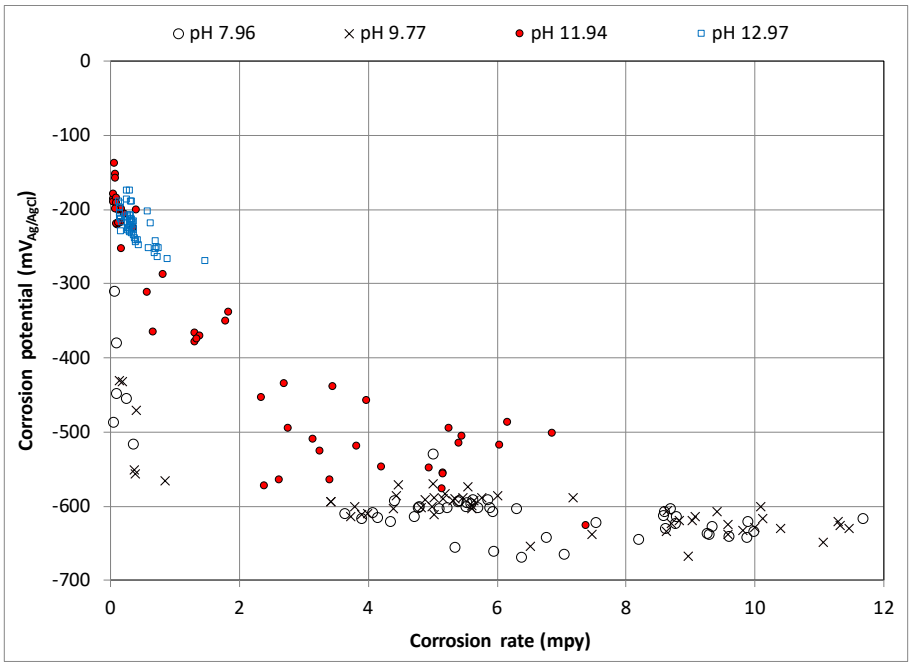

Source: FHWA.

Figure 40. Graph. Relationship between corrosion rate data and corrosion potential data from Batch #2 in different pH solutions containing all [SO_4^{2-}].

Again, this scatter plot clearly shows that the corrosion behavior of the wires in the sulfate solutions, represented by corrosion rate and corrosion potential, largely depended on pH. At higher pH, corrosion rates were lower and corrosion potentials were more positive. As observed previously, sulfate-free solutions exhibited a wide range of corrosion potential (figure 33 and figure 34) depending on pH. Still, all the corresponding corrosion rates were very low.

CHARACTERISTICS OF GROUT SAMPLES

Physical Appearance of Fresh Grout

When Product 1 and Product 2 were mixed with their recommended amounts of water, the fresh mixes looked normal. A representative fresh grout mix of Product 1 is shown in figure 41.

Source: FHWA.

Figure 41. Photo. Fresh grout mix of a Product 1 specimen.

However, the fresh grout mix of #1 Old Product 3 exhibited an unusual appearance, even though the recommended water dosage was used. Soon after the mix was poured into the mold, unidentified black particles and many tiny air bubbles surfaced along the mold's rim. Petrographic examination later identified the floating black particles as silica-fume agglomerates. Figure 42 shows a fresh mix made with #1 Old Product 3.

Source: FHWA.

Figure 42. Photo. Fresh grout mix of a #1 Old Product 3 specimen.

Figure 43 shows the worsened condition of the fresh mix shown in figure 42 after adding 0.5 lb of water.

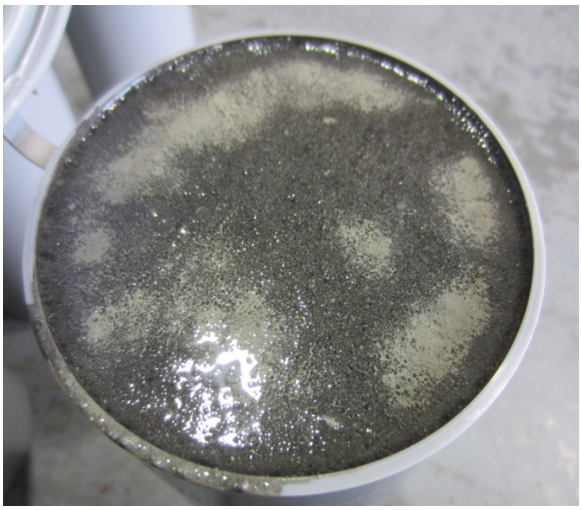

Source: FHWA.

Figure 43. Photo. Fresh grout mix of another #1 Old Product 3 specimen after adding 0.5 lb of extra water to the fresh mix shown in figure 42.

Figure 44 and figure 45 show fresh mixes of the #2 Old Product 3 made with the recommended water content and with an extra 0.5 lb of water to the leftover fresh mix, respectively.

Source: FHWA.

Figure 44. Photo. Fresh grout mix of a #2 Old Product 3 specimen made with the recommended water dosage.

Source: FHWA.

Figure 45. Photo. Fresh grout mix of another #2 Old Product 3 specimen after adding 0.5 lb of extra water to the fresh mix shown in figure 44.

Unlike #1 Old Product 3, #2 Old Product 3 did not exhibit excessive silica-fume particles. However, regardless of the amount of mixing water, the #2 Old Product 3 that had been kept in an opened bag produced the most significant amounts of silica-fume particles and air bubbles observed in this study. Figure 46 shows a fresh mix using the recommended water dosage, and figure 47 shows another fresh mix after adding an extra 0.5 lb of water to the leftover fresh mix shown in figure 46.

Source: FHWA.

Figure 46. Photo. Fresh grout mix of a #2 Old Product 3 (opened bag) specimen made with the recommended water dosage.

Source: FHWA.

Figure 47. Photo. Fresh grout mix of another #2 Old Product 3 (opened bag) specimen after adding 0.5 lb of extra water to the fresh mix shown in figure 46.

It is unclear why the grout in the opened bag yielded more black particles and air bubbles than the same material in the sealed bags.

Physical Appearance of Hardened Grout

Figure 48 shows the hardened surfaces of Product 1 specimens.

Source: FHWA.

Figure 48. Photos. Surface conditions of Product 1 specimens.

The Product 1 specimens mixed with the recommended amount of water (P1-1 through P1-3) showed a dark gray color. The top surface of the extra-water specimen (P1-4) appeared to be porous and of a slightly lighter gray color than the others, presumably due to segregation in the presence of excessive water. Table 7 lists the water-soluble sulfate concentrations in the raw grout, top surface layer, and body of the hardened Product 1 grout specimens.

Table 7. [SO_4^{2-}] concentration in Product 1 specimens (percent by weight of sample).

Sample ID	Raw Grout Powder	Top Layer	Mean of Top/M/B Sections
P1-1	1.01	0.48	0.10
P1-2	0.92	0.90	0.09
P1-3	0.83	1.07	0.07
P1-4	0.83	0.09	0.06

ID = identifier; M = middle; B = bottom.

Figure 49 shows the hardened surface conditions of Product 2 specimens.

Source: FHWA.

Figure 49. Photos. Surface conditions of Product 2 specimens.

The top surfaces of Product 2 specimens showed a light gray color except for P2-3, which exhibited darker gray in the wetted area. The extra-water specimen (P2-4) also exhibited a porous top surface due to segregation in the presence of excessive water. Table 8 lists the water-soluble sulfate concentrations in the raw grout, top surface layer, and body of the hardened Product 2 grout specimens.

Table 8. [SO_4^{2-}] concentration in Product 2 specimens (percent by weight of sample).

Sample ID	Raw Grout Powder	Top Layer	Mean of Top/M/B Sections
P2-1	0.54	0.17	0.09
P2-2	0.90	0.09	0.09
P2-3	0.63	0.06	0.05
P2-4	0.63	0.09	0.09

ID = identifier; M = middle; B = bottom.

Figure 50 shows the hardened surface conditions of the #1 Old Product 3 specimens.

Source: FHWA.

Figure 50. Photos. Surface conditions of #1 Old Product 3 specimens.

The hardened specimens made with #1 Old Product 3 exhibited exceptionally porous top surfaces containing many air bubbles of different sizes. As far as physical appearance was concerned, #1 Old Product 3 was judged to be the worst among the grout materials tested in this study. The color variation was also the largest. If the condition of #1 P3-4 is compared with its fresh mix condition, shown in figure 43, it can be speculated that black particles floated continuously to the top and formed a relatively thick, porous deposit layer, even during the plastic stage of the mix. The age of the grout, long past its indicated shelf life, may have been responsible for the selective leaching of silica-fume particles and numerous air bubbles through intense grout segregation process. Table 9 lists the water-soluble sulfate concentrations in the raw grout, top surface layer, and body of the hardened #1 Old Product 3 grout specimens.

Table 9. [SO_4^{2-}] concentration in #1 Old Product 3 specimens (percent by weight of sample).

Sample ID	Raw Grout Powder	Top Layer	Mean of Top/M/B Sections
#1 P3-1	0.38	0.05	0.08
#1 P3-2	0.93	0.14	0.10
#1 P3-3	0.56	0.20	0.11
#1 P3-4	0.56	0.39	0.10

ID = identifier; M = middle; B = bottom.

Figure 51 shows the hardened surface conditions of the #2 Old Product 3 specimens.

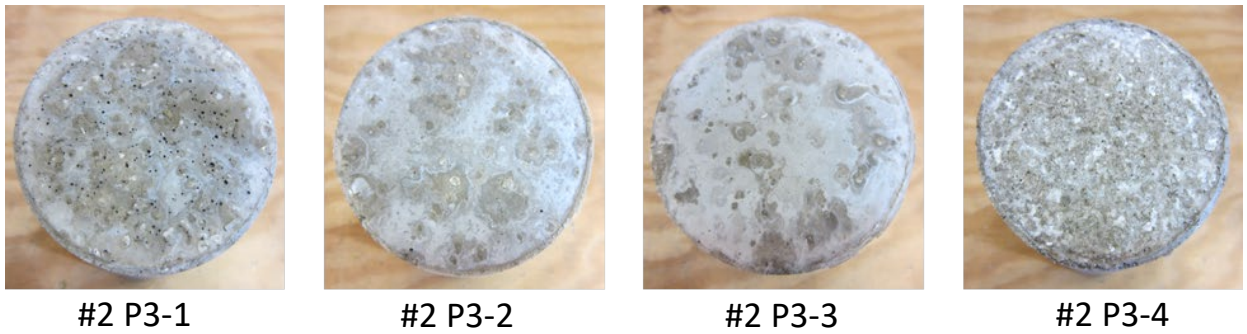

Source: FHWA.

Figure 51. Photos. Surface conditions of #2 Old Product 3 specimens.

The color of the hardened specimens made with #2 Old Product 3 was light gray. The most porous top surface (#2 P3-4) was caused by grout segregation in the presence of excessive water. If the hardened surface conditions of #2 P3-3 and #2 P3-4 are compared with their fresh-mix conditions, shown in figure 44 and figure 45, it is clear that no drastic changes occurred during the setting and curing periods. Table 10 lists the water-soluble sulfate concentrations in the raw grout, top surface layer, and body of the hardened #2 Old Product 3 grout specimens.

Table 10. [SO_4^{2-}] concentration in #2 Old Product 3 specimens (percent by weight of sample).

Sample ID	Raw Grout Powder	Top Layer	Mean of Top/M/B Sections
#2 P3-1	0.83	0.22	0.12
#2 P3-2	0.35	0.71	0.11
#2 P3-3	0.67	0.41	0.12
#2 P3-4	0.67	0.42	0.12

ID = identifier; M = middle; B = bottom.

Figure 52 shows the hardened surface conditions of #2 Old Product 3 specimens made with the leftover grout in the opened bag.

Source: FHWA.

Figure 52. Photos. Surface conditions of #2 Old Product 3 specimens (opened bag).

The #2 Old Product 3 (opened bag) specimen mixed with the recommended amounts of water (#2 P3-5) exhibited a denser top surface than the one with extra water (#2 P3-6). The top surfaces of both specimens formed thick black deposit layers, an outcome consistent with their fresh mixes, which had exhibited silica-fume particles with numerous bubbles (figure 46 and figure 47). The product's age (several years past expiration) and its prolonged exposure to moisture in the air must have contributed to the specimens' unusual condition, which was drastically different from the condition of the specimen made with the same material in the sealed bags. Table 11 lists the water-soluble sulfate concentrations in the raw grout, top surface layer, and body of the hardened #2 Old Product 3 (opened bag) grout specimens.

Table 11. [SO_4^{2-}] concentration in #2 Old Product 3 specimens (opened bag) (percent by weight of sample).

Sample ID	Raw Grout Powder	Top Layer	Mean of Top/M/B Sections
#2 P3-5	0.84	0.46	0.12
#2 P3-6	0.84	0.41	0.11

ID = identifier; M = middle; B = bottom.

Comparing the physical appearances of the hardened grout specimens from a material standpoint shows that, to minimize the risk of producing deficient grout in the field, it is essential to observe the following guidelines when using PTI Class C prepackaged grout products:

- Store the grout in the field according to the manufacturer's recommendation.
- Use the grout within the manufacturer's specified shelf life.
- Add mixing water according to the manufacturer's recommendation.

Petrographic Examination and Chemical Analyses

The following presents excerpts of the petrographic analysis report. The full report is included in the appendix.

Raw Grout Powder

The raw grout sample consisted of loose gray powder with many ovoid lumps that could be easily broken apart. Microscopy examination of the sample revealed that recognizable components (particles larger than approximately 0.2 mil) of the loose powder made up approximately 90 percent of the total sample and consisted of approximately 60 to 65 percent portland cement, 30 percent fragmental carbonate (interground limestone), 3 to 5 percent anhydrite (anhydrous calcium sulfate), 3 percent calcium aluminate cement, 1 to 2 percent silica-fume agglomerates, and a trace amount (less than 1 percent) gypsum (i.e., calcium sulfate dihydrate).

The maximum size of the portland cement particles and carbonate fragments was 4.7 mil. Anhydrite crystals in the 4- to 8-μm size range were common. No large particles of gypsum or plaster (calcium sulfate hemihydrate) were observed. Silica-fume agglomerates were mostly 0.4 to 2.0 mil in diameter. Approximately 10 percent of particles in the sample were less than 0.2 mil in diameter. Anhydrite, carbonate, and cementitious fines (portland cement, calcium aluminate cement, and silica fume) were among the particles that were less than 0.2 mil in diameter.

Supplementary cementitious materials, such as fly ash or slag cement, and particles that could be interpreted as dry organic admixtures were not observed. However, the grout powder also contained substantial amounts of particles that were too small to be resolved and identified using optical methods. The sulfate was contained in these fine particles, smaller than 5 μm of the raw grout powder. Sulfate minerals were typically soft and may have constituted a major portion of the particles smaller than a No. 325 sieve (1.772 mil) when the sulfate mineral was interground with substantially harder cement clinker.

The composition of the ovoid lumps was generally similar to that of the loose powder. Silica-fume agglomerates tended to be larger in the ovoid lumps, and a few agglomerates were 1.181 to 1.969 mil in diameter. Many cement particles exhibited thin, partial films of hydration products where multiple particles were in contact, indicating that the sample might have experienced limited hydration caused by exposure to ambient moisture.

Hardened Laboratory Grout Samples

Sample #1 P3-2M, made with #1 Old Product 3, generally exhibited a uniform distribution of constituents in the hardened grout. Most air voids did not exhibit linings or coatings. The dark material in the occasional air voids was visually consistent with silica fume. The lined voids might have formed by plucking hard silica-fume agglomerates during cutting. The paste was typically carbonated around air voids and microcracks, and patchy carbonation was observed throughout the grout. Microcracks were infrequent, narrow, and empty. Fragmental carbonate particles up to 19.7-mil long were the principal aggregates in the grout (55 to 65 percent by volume). Quartz aggregate particles made up approximately 1 to 2 percent of the aggregate. Aggregate distribution was generally uniform. No evidence of deleterious behavior was observed. The paste contained silica-fume agglomerates (1 to 2 percent by volume of paste), residual unhydrated, and partially hydrated portland cement particles (6 to 8 percent by volume of paste), and calcium aluminate cement particles (2 percent by volume of paste).

Another hardened grout, Sample #1 P3-4 xtra T, made with additional water, exhibited a greater paste-to-aggregate ratio. It contained more frequent shrinkage cracks compared to Sample #1 P3-2M, which contained the recommended water dosage. The constituents were non-uniformly distributed on a microscale. Overall, the extent of portland cement hydration was greater, and many partially hydrated portland cement particles exhibited substantial hydration rims.

Both hardened laboratory samples contained fragmental carbonate (identified by XRD as calcite and dolomite), portland cement, silica-fume agglomerates, and a small amount of calcium aluminate cement.

Segregated Field Sample

The hard portion of the segregated field grout sample appeared to have a well-consolidated, uniform surface, no corrosion products, and no other secondary deposits. The broken surfaces were uniform in appearance and showed characteristics of subconchoidal fracture (smooth and nearly shell-shaped). No macroscale cracks or unusual characteristics were observed. Silica-fume agglomerates were not observed.

The soft portion of the segregated field grout sample exhibited a dark color due to moisture retention. The fragments became lighter in color as the material air dried. The dried material developed desiccation cracks. Patches of red-brown corrosion products were commonly observed and were typically associated with white chalky material and light gray, semitranslucent material. The sample contained a small number of hard, light gray grout fragments. Silica-fume agglomerates were not visible at 5 to 50× magnifications.

XRD analysis, total sulfur content, and water-soluble sulfate content tests were performed on Sample #1 P3-2M and the hard and soft portions of the field sample. None of the analyzed samples contained a sulfate mineral as a major component. Ettringite was identified as a minor or trace component of each sample and is an expected hydration product of portland cement. Gypsum was identified as a possible trace component of the hard portion of the field sample.

The total sulfur content of the soft portion of the field sample was more than five times that of the hard portion of the sample and more than 3.5 times that of Sample #1 P3-2M. The total sulfur content in Sample #1 P3-2M likely represents the actual available sulfur in the grout. The water-soluble sulfate content in Sample #1 P3-2M and the hard portion of the field sample were virtually the same. However, the water-soluble sulfate content of the soft portion of the field sample was 100 times that of the other samples (29,970 ppm versus 340 ppm (#1 P3-2M) and 270 ppm (hard field sample)). Water-soluble sulfate was concentrated in the pore solutions, and sulfate would be strongly partitioned into the water-rich portion of the segregated grout.

CONCENTRATION OF WATER-SOLUBLE SULFATE IONS IN GROUT SAMPLES

Figure 53 summarizes the mean water-soluble sulfate concentration data listed in table 7 through table 11.

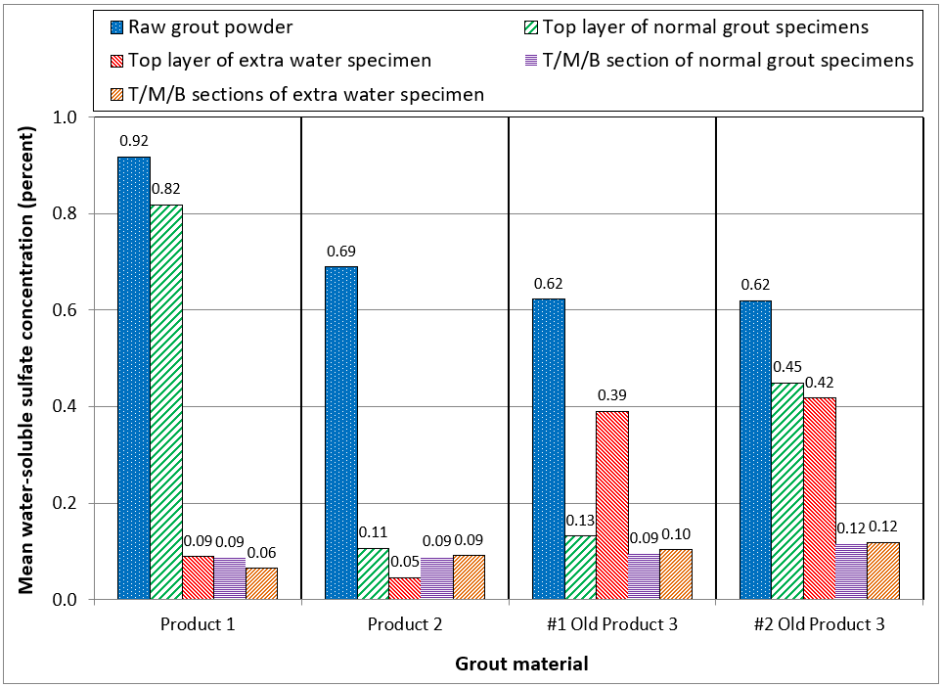

Source: FHWA.
T = top; M = middle; B = bottom.

Figure 53. Graph. Mean water-soluble sulfate concentration data in various types of grout samples.

Water-soluble sulfate concentration in the raw grout powders ranged from 0.35 to 1.01 percent by weight of sample. Product 1 contained the highest mean concentration (0.92 percent) in the three bags. Product 2 and Product 3 had similar mean concentrations (0.69 and 0.62 percent, respectively).

When the raw grout powders were mixed with water and cured, most of the water-soluble sulfate became bound to the hardened grout through the hydration process. The sulfate content of individual sections, as well as the mean sulfate content of the three hardened grout sections (top/middle/bottom), were consistently reduced to around 0.1 percent, which is about 12 percent

of raw Product 1 powder and 20 percent of the other products. The same reduction was observed in the extra-water specimens.

Product 2 showed an excellent binding capability, with significantly reduced water-soluble sulfate in the hardened grout, regardless of the sampling location and amount of mixing water. Product 3 released more sulfate (0.39 and 0.42 percent) in the thin top layer (presumably segregated) than the other products when excessive water was used. Product 1 and #2 Old Product 3 were determined to have the two highest mean concentrations (0.82 and 0.45 percent) in the thin top layers of the specimens made with the recommended water quantity. However, #1 Old Product 3 had 0.13 percent water-soluble sulfate in the top layer.

Table 12 lists the water-soluble sulfate concentrations of the FHWA chloride threshold study specimens.[12]

Table 12. Water-soluble sulfate analysis results from the FHWA study.

Sample ID	Sample Weight (oz)	Percent by Grout Weight
Black particles collected from void/grout interface of 0 percent chloride specimen	0.071	1.5
Top layer scraped from void/grout interface of 0 percent chloride specimen	0.176	1.5
Top layer scraped from void/grout interface of 0.2 percent chloride specimen	0.176	0.4
Top layer scraped from void/grout interface of 0.4 percent chloride specimen	0.176	0.1
Grout powder sample from 0 percent chloride specimen	0.071	0.0
Grout powder sample from 0.08 percent chloride specimen	0.071	0.1
Grout powder sample from 0.4 percent chloride specimen	0.071	0.0
Raw grout powder	0.176	0.5

ID = identifier.

Since the #2 Old Product 3 specimens were made with the same grout used for the FHWA chloride threshold study, two groups of sulfate data are compared here. The expired Product 3 powder had 24 percent more water-soluble sulfate than the same grout powder used within its shelf life (0.62 percent versus 0.50 percent by weight of sample). The highest water-soluble sulfate concentration in the segregated top layers of the old grout specimens was 3.5 times (1.5 percent versus 0.42 percent) greater than those in the same areas of the unexpired grout specimens. Differences in the degree of grout segregation and, more importantly, the age of the grout powder may have contributed to the discrepancy. However, both sets of sulfate data clearly indicate that a high level of water-soluble sulfate can be found in the segregated top layers.

The petrographic examination and chemical analyses of the field grout samples indicated that the excessive water-soluble sulfate was more often found in the pore solutions and water-rich, soft segregated grout sample than in the hard, dried grout sample. The total sulfur content of the soft field grout sample was also 3.5 to 5 times that of the hardened field grout sample. Water-soluble sulfate ions can likely migrate through water movement as part of the grout segregation process, and these active anions are concentrated in the soft segregated grout sample. When the deficient grout is carbonated, augmented by moist grout condition, water-soluble sulfate ions become aggressive, as observed previously in the low-pH aqueous solutions. However, it is still unclear under what condition(s) the segregated grout becomes soft, containing excessive water-soluble sulfate ions.

DISCUSSION

The prepackaged grout products acquired for this study did not possess a uniform and consistent quality in terms of bag weight, water-soluble sulfate concentration in the raw powder and the hardened grout, and characteristics of fresh mix. Because a bag can weigh less than its nominal posted weight, using the recommended water content may actually result in an excessively hydrated mix. This is problematic because grout segregation will likely occur at the job site.

Segregated grout is also a negative consequence of the complex interactions among parameters other than excessive mixing water, including individual raw ingredients, the mixing and pumping process, bleeding, curing, and tendon profile. Even when prepared in a reasonably controlled environment, laboratory specimens displayed different degrees of grout segregation and, consequently, sometimes a high level of water-soluble sulfate was released into the segregated grout.[(12)]

There was no apparent relationship between the content of water-soluble sulfate in raw grout materials and the content in segregated grout, especially in the topmost layer. Also, the visual appearance of fresh grout mix could not be correlated with how much water-soluble sulfate was released after segregation. However, it was apparent that the aged/expired raw grout was more prone to segregation and thus readily released water-soluble sulfate into the segregated grout. Furthermore, the petrographic examination and chemical analyses revealed that water-soluble sulfate migrated toward areas with more moisture. Pore water and soft/wet segregated grout retained 100 times the water-soluble sulfate and more than five times the total sulfur content than dried and hardened grout did.

The test results show that, if the segregated grout maintains a low-pH environment by carbonation, the water-soluble sulfate ions accumulated there become as aggressive as water-soluble chloride ions. Also, the silica-fume agglomerates and air bubbles in various sizes can form a porous, black deposit layer over the segregated top surface, which can hold water for an extended period of time. Under these conditions, water-soluble sulfate ions can induce significant corrosion damage, as observed in the FHWA study, *Post-Tensioning Tendon Grout Chloride Thresholds*.[(12)]

CHAPTER 5. CONCLUSIONS

Based on the test results obtained from the 6-mo accelerated corrosion study and examination of various grout samples, the following conclusions can be drawn:

- In low-pH aqueous solutions (8.0 and 10.0) that simulated carbonated bleed water and grout pore water, water-soluble sulfate ions behaved like chloride ions in terms of instantaneous corrosion rate (indicative of corrosion kinetics), corrosion potential (indicative of corrosion tendency), and degree of pitting resistance. This means that sulfate is as detrimental to PT strands as chloride if the strands are not protected by high-pH grout. However, in high-pH aqueous solutions (12.5 and 13.6), sulfate was less corrosive than chloride. Although this study could not determine the sulfate threshold for corrosion, it was found that sulfate content as low as 0.05 percent at neutral pH could initiate corrosion, and 0.4 percent sustained corrosion activities. When chloride and sulfate of equal concentrations coexisted in different pH aqueous solutions, chloride was the dominant species in determining the corrosivity of the solutions.

- Water-soluble sulfate ions also showed temperature-dependent corrosivity similar to that of the chloride ions observed in the FHWA chloride threshold study. Corrosion was more severe at the elevated temperature (104 °F) than at the ambient temperature (77 °F). Specifically, as the anion concentration increased in any pH solution, the corrosion rate of the center wires did not increase proportionally from that of the anion-free condition at the ambient temperature but jumped significantly at the elevated temperature. Mean corrosion rates at 32 °F were less than 10 percent of those measured at the ambient temperature, regardless of sulfate concentration.

- The content of water-soluble sulfate in raw grout powders ranged from 0.35 to 1.01 percent by weight of sample. When the grout powders were mixed with water and cured, most of the sulfate became bound to the hardened grout and water-soluble sulfate was reduced to 0.1 percent. Segregated grout is a negative consequence of the complex interactions among many parameters, including individual raw ingredients, an excess amount of mixing water, the mixing and pumping process, bleeding, curing, and tendon profile. Aged/expired raw grout was more prone to segregation and thus readily released water-soluble sulfate ions into the segregated grout.

- Petrographic examination and chemical analyses revealed that pore water and soft/wet segregated grout retained 100 times the water-soluble sulfate and more than five times the total sulfur content than dried and hardened grout did. This is because water-soluble sulfate ions can migrate via water movement toward areas with more moisture. If the segregated grout maintains a low-pH environment by carbonation, the water-soluble sulfate ions accumulated there become as aggressive as chloride ions. Also, silica-fume agglomerates and air bubbles in various sizes can form a porous black deposit layer over a segregated top surface and hold moisture for an extended period. As a result, corrosion can be initiated on a strand in direct contact with a carbonated layer of segregated grout with a concentration of water-soluble sulfate ions as low as 0.05 percent by weight of sample.

APPENDIX. LABORATORY STUDIES OF FIVE PTI CLASS C GROUT SAMPLES

INTRODUCTION

Researchers analyzed a raw grout powder, a grout sample obtained from a post-tensioned duct of the Ringling Causeway Bridge in Sarasota Bay, Florida, and other grout samples made with a PTI Class C grout.[16] Their assessment focused on identifying potential sources of water-soluble sulfate (which may play a role in initiating corrosion in post-tensioned strands) in the raw grout and investigating grout segregation in the samples. Table 13 describes each sample and the tests performed on it.

Table 13. Grout samples and testing program.

Sample ID	Description	Source	Testing Performed
#1 P3-2M #1 P3-2B	Mixed-in-the-lab, hardened grout with 12.5 lb of water added per 50-lb bag, with samples taken from the middle section of a 4- by 8-inch cylinder (#1 P3-2M) and the bottom section of a 4- by 8-inch cylinder (#1 P3-2B)	#1 Old Product 3 acquired in 2009	XRD, total-sulfur element analysis, ASTM C1580 water-soluble sulfate, and thin-section microscopy (to compare samples with #1 P3-4 xtra T)
#1 P3-4 xtra T	Mixed-in-the-lab, hardened grout with an extra 0.5 lb of water added to the #1 P3-2 mix after casting three cylinders	#1 Old Product 3 acquired in 2009	Thin-section microscopy (to compare sample with #1 P3-2M and #1 P3-2B)
Raw	#1 Old Product 3 grout powder sampled 10/13/2015	#1 Old Product 3 acquired in 2009	microscopy
403-6L	Soft and hardened segregated grout from a high point of an external tendon	Ringling Causeway Bridge, completed in 2003	Brief microscopy, XRD, total-sulfur element analysis, and ASTM C1580 water-soluble sulfate

ID = identifier; M = middle; B = bottom.

SAMPLE DESCRIPTIONS

Each sample was examined visually and with a stereomicroscope in accordance with the pertinent sections of ASTM C856, which also applies to grout.[17]

Samples #1 P3-2M and #1 P3-2B

Samples #1 P3-2M and #1 P3-2B, shown in figure 54 through figure 58, consisted of two saw-cut sections of light gray grout that had been cast in a 4-inch diameter cylindrical mold. Sample #1 P3-2M, the smaller section, was a 0.8-inch-thick, saw-cut, half-slice sample cut from the middle of the larger sample. Sample #1 P3-2B, the larger section, was a 2.3-inch-thick, full-cylindrical sample cut from the bottom of the sample. The saw-cut surfaces of both samples were examined using a stereomicroscope to assess the distribution of constituents. Samples #1 P3-2M and #1 P3-2B were visually similar and appeared generally uniform. Both samples contained white carbonate aggregate particles up to 0.025 inch in diameter and black silica-fume agglomerates up to 0.015 inch in diameter. The saw-cut surfaces exhibited frequent air bubbles up to 0.09 inch in diameter. The interior surface of the air voids often had a thin, black lining. Optical characteristics of the black material were consistent with silica fume.

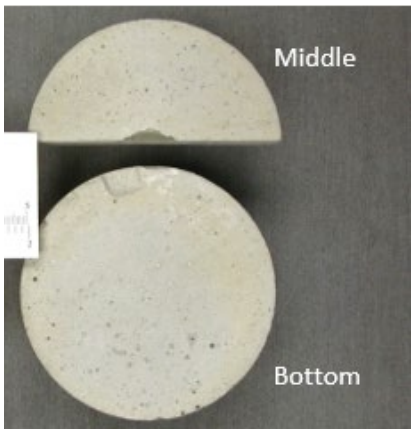

Source: FHWA.

A. Top view.

Source: FHWA.

B. Side view.

Figure 54. Photos. Middle and bottom slices from Sample #1 P3-2.

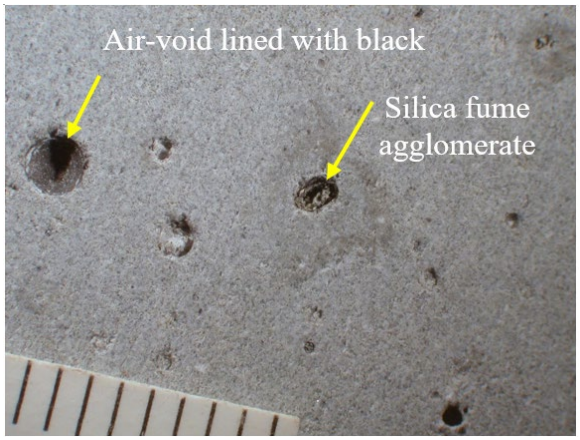

Source: FHWA.

Figure 55. Photo. Stereomicroscope view (millimeter scale) of the saw-cut surface of Sample #1 P3-2B.

Source: FHWA.

Figure 56. Photo. Stereomicroscope view (millimeter scale) of the saw-cut surface of Sample #1 P3-2M showing a thin film of black material in the air voids.

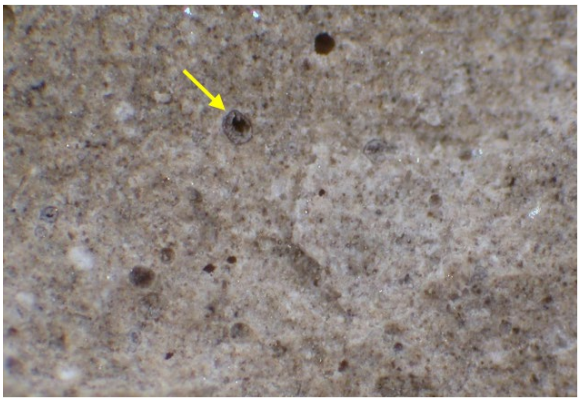

Source: FHWA.

Figure 57. Photo. Sample #1 P3-2M at 25× magnification showing white particles and dark silica-fume agglomerates (arrow) on the fracture surface.

Source: FHWA.

Figure 58. Photo. Sample #1 P3-2M at 15× magnification showing white particles and dark silica-fume agglomerates (arrow) on the fracture surface.

Sample #1 P3-4 xtra T

Sample #1 P3-4 xtra T, shown in figure 59 through figure 63, consisted of one-half of a 0.8-inch thick, transverse slice of light gray grout that had been saw-cut from the top of a 4-inch-diameter cylinder. The top surface was generally flat and was covered with small craters formed by burst air or gas bubbles and small gray to black silica-fume agglomerates. Crater floors were thinly coated with a black film similar to the black film observed in air voids in Sample #1 P3-2M. Patches of white, blue-white, and colorless alkali–silica reaction (ASR) gel were frequently observed in the craters, further suggesting that the black film is silica fume. The saw-cut transverse and vertical surfaces were examined using a stereomicroscope to assess the distribution of constituents. The surfaces were similar to the saw-cut surfaces described for both samples #1 P3-2M and #1 P3-2B.

Source: FHWA.

A. Top surface.

Source: FHWA.

B. Saw-cut bottom surface.

Figure 59. Photos. Sample #1 P3-4 xtra T.

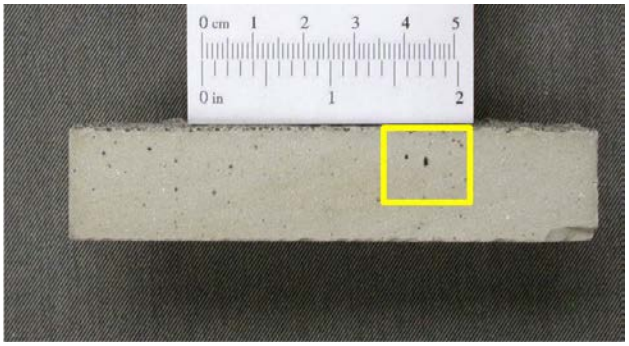

Source: FHWA.

Figure 60. Photo. Vertical saw-cut side of Sample #1 P3-4 xtra T (region in box is shown in figure 71).

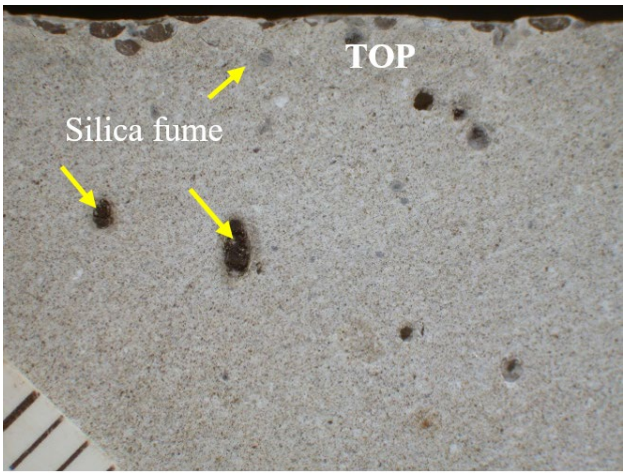

Source: FHWA.

Figure 61. Photo. Close-up view (millimeter scale) of the vertical cross section of Sample #1 P3-4 xtra T showing craters at the top.

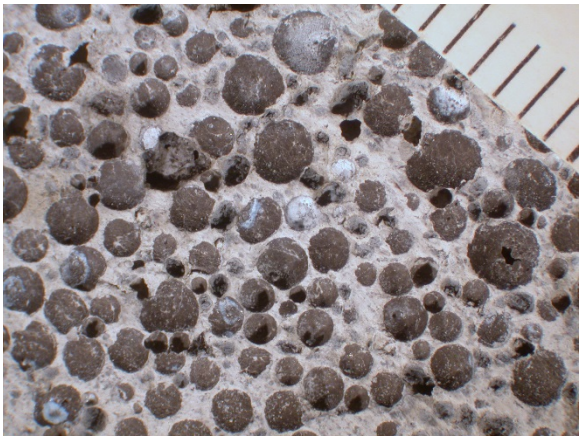

Source: FHWA.

Figure 62. Photo. Close-up view (millimeter scale) showing craters on the top surface of Sample #1 P3-4 xtra T.

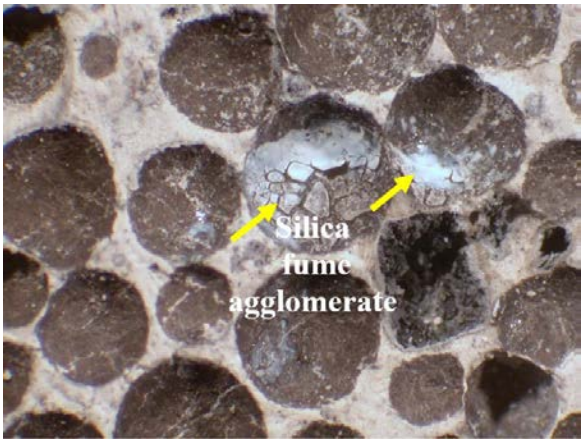

Source: FHWA.

Figure 63. Photo. Sample #1 P3-4 xtra T at approximately 25× magnification showing ASR gel and silica-fume agglomerates in craters.

Raw Grout Sample

The raw grout sample, shown in figure 64 through figure 70, consisted of 2.8 lb of loose, gray powder that contained frequent ovoid lumps that could easily be broken apart. Immersion preparations were made by mixing immersion media with refractive index 1.54, a small amount of the loose powder, and a small amount of a crushed ovoid lump. The recognizable components of the loose powder made up approximately 90 percent of the total sample and consisted of approximately 60 to 65 percent portland cement, 30 percent fragmental carbonate (interground limestone), 3 to 5 percent anhydrite (anhydrous calcium sulfate), 3 percent calcium aluminate cement, 1 to 2 percent silica-fume agglomerates, and a trace amount (less than 1 percent)

gypsum. The maximum size of the portland cement particles and carbonate fragments was 120 µm. Anhydrite crystals in the 0.16 to 0.315 mil size range were common. No large particles of gypsum (calcium sulfate dihydrate) or plaster (calcium sulfate hemihydrate) were observed. Silica-fume agglomerates were mostly 0.394 to 1.969 mil in diameter. The sample contained approximately 10 percent particles that were less than 0.197 mil in diameter and, as a result, these particles could not be positively identified by optical microscopy. Anhydrite, carbonate, and cementitious fines (portland cement, calcium aluminate cement, and silica fume) were among the particles that were less than 5 µm in diameter. No supplementary cementitious materials, such as fly ash or slag cement, were observed. Since fly ash and slag cement particles are normally similar in size to portland cement particles, they should have been identifiable using optical microscopy. No particles that could be interpreted as dry organic admixtures were observed.

The composition of the ovoid lumps was generally similar to that of the loose powder. The recognizable components of the lumps consisted of approximately 70 percent portland cement, 25 percent fragmental carbonate (interground limestone), 2 to 3 percent silica-fume agglomerates, and trace amounts of anhydrite, gypsum, and partially carbonated calcium hydroxide. Silica-fume agglomerates tended to be larger in the ovoid lumps, and a few were 30 to 50 µm in diameter. Many cement particles exhibited thin, partial films of hydration product where multiple particles were in contact. The appearance of the sample indicated it may have experienced limited hydration caused by exposure to ambient moisture.

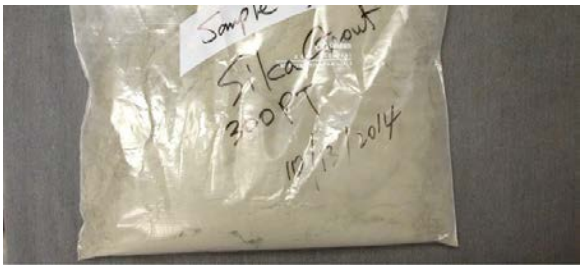

Source: FHWA.

Figure 64. Photo. Raw grout sample.

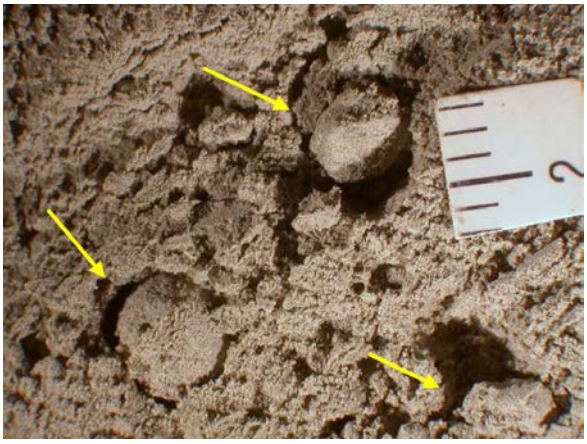

Source: FHWA.

Figure 65. Photo. Stereomicroscope micrograph (millimeter scale) showing ovoid lumps in the raw grout sample.

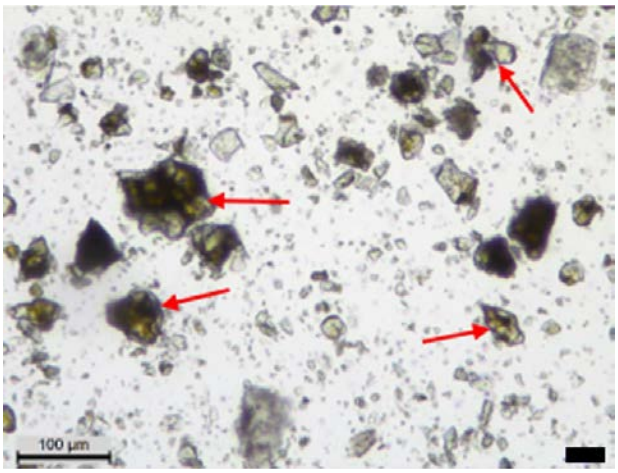

Source: FHWA.

A. Plane-polarized light on portland cement particles (arrows).

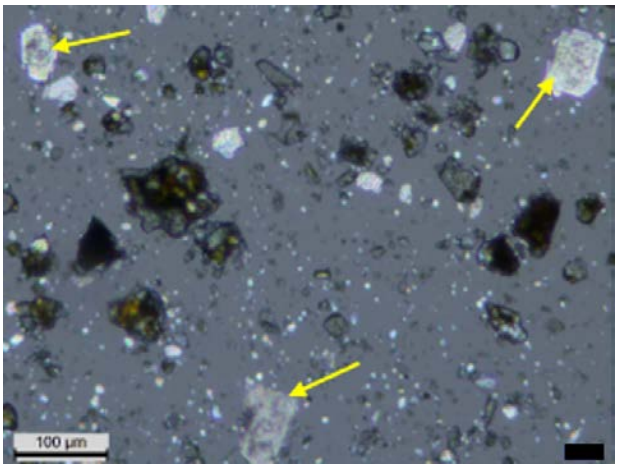

Source: FHWA.

B. Cross-polarized light on fragment carbonate (arrows).

Figure 66. Photos. Major constituents of the raw grout sample.

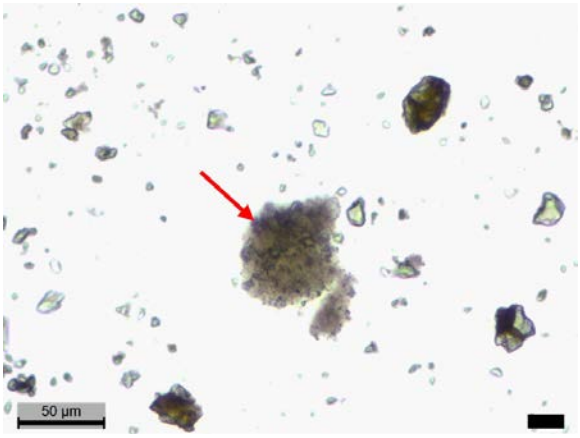

Source: FHWA.

Figure 67. Photo. Plane-polarized light on silica-fume agglomerate in the raw grout sample powder.

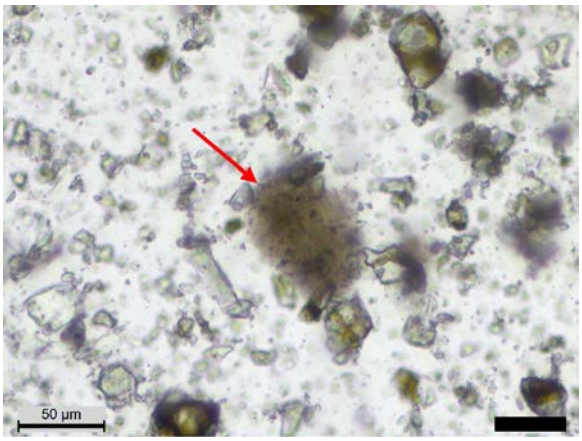

Source: FHWA.

Figure 68. Photo. Plane-polarized light on silica fume agglomerate in a raw grout sample ovoid lump.

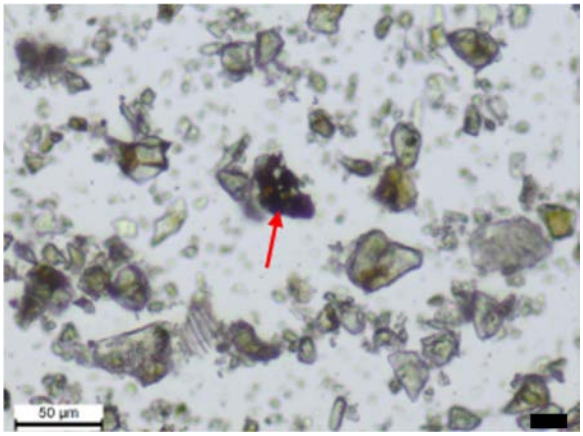

Source: FHWA.

Figure 69. Photo. Plane-polarized light on a calcium aluminate cement particle (red arrow) in the raw grout sample.

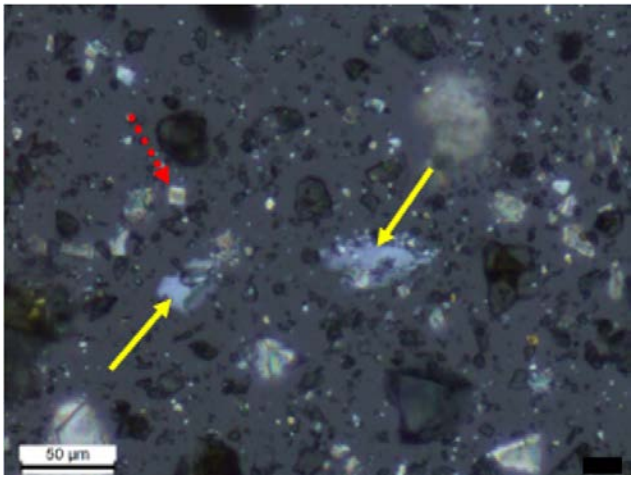

Source: FHWA.

Figure 70. Photo. Thin-section micrograph showing examples of anhydrite (red dash line arrow) and gypsum (yellow solid line arrows) in the raw grout sample.

Field Sample

The field sample, shown in figure 71 through figure 74, was provided in two bags: one bag contained three hard fragments of medium gray grout and the other contained smaller fragments of soft, moist grout. The hard fragments were approximately 1 inch wide and 1.5 to 3 inches long. The surface that had been in contact with the duct was curved, smooth, and exhibited small air-bubble craters. The surface that had been in contact with the strand was well consolidated, uniform in appearance, and free of corrosion deposits and other secondary deposits. The broken surfaces were uniform in appearance and the character of the fracture was subconchoidal (smooth and nearly shell-shaped). No macroscale cracks or unusual characteristics were observed. Silica-fume agglomerates were not observed.

Source: FHWA.

A. Surfaces in contact with the duct.

Source: FHWA.

B. Surfaces with the strand imprints.

Figure 71. Photos. Hard fragments from the field sample.

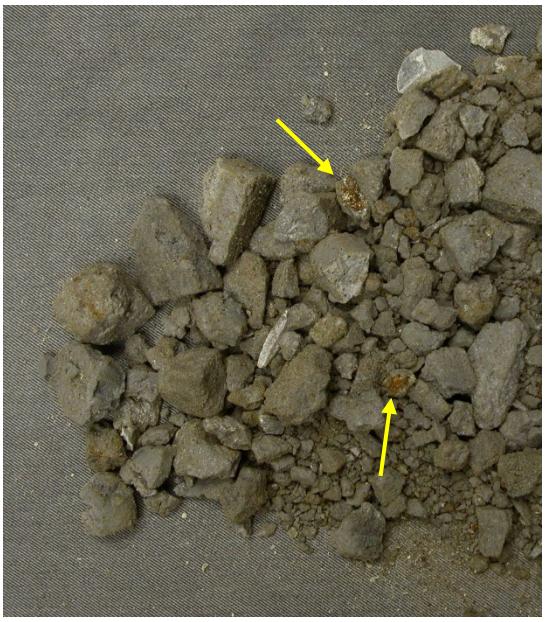

Source: FHWA.

Figure 72. Photo. Soft material from the field sample.

The dark color of the soft material was caused by moisture retention. The fragments became lighter in color and developed desiccation cracks as the material air dried (figure 73). Patches of red-brown corrosion deposits were commonly observed and were typically associated with the white chalky and light gray, semitranslucent materials (indicated by yellow arrows in figure 72 and figure 74). The sample contained a small number of hard, light gray grout fragments. Silica-fume agglomerates were not visible at 5 to 50× magnifications.

Source: FHWA.

Figure 73. Photo. Field sample at approximately 10× magnification showing examples of desiccation cracks in air-dried soft grout.

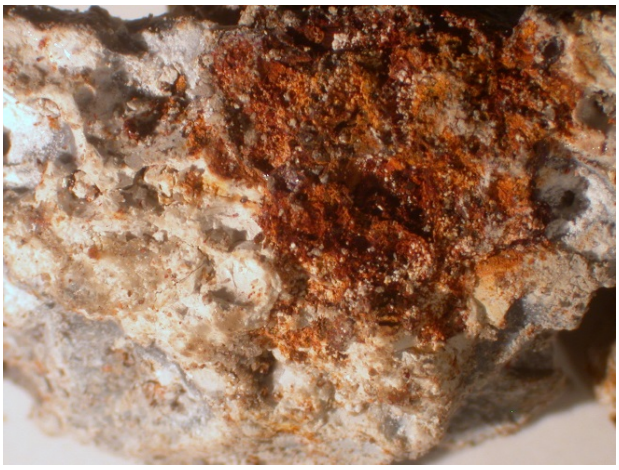

Source: FHWA.

A. On chalky material.

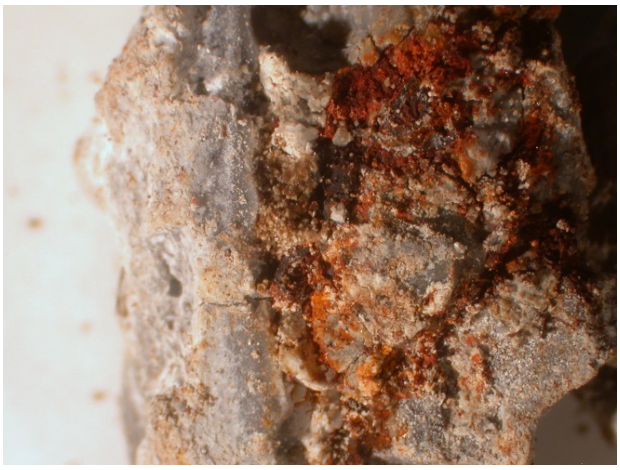

Source: FHWA.

B. On light gray, semitranslucent material.

Figure 74. Photos. Field sample showing examples of corrosion deposits.

COMPARATIVE MICROSCOPY OF GROUT

Researchers performed detailed thin-section analyses on grout that had reportedly been mixed with 12.5 lb of water per 50-lb bag (Sample #1 P3-2M) and grout that had been mixed with additional water (Sample #1 P3-4 xtra T). Both samples contained silica-fume agglomerates and air voids that were lined with silica fume.

Sample #1 P3-2M

The Sample #1 P3-2M grout generally exhibited a uniform distribution of constituents, but microscale variations were frequently observed. Most air voids did not exhibit linings or coatings (figure 75). The dark material in the occasional air voids that did exhibit linings was optically consistent with silica fume (figure 76). The lined voids may have formed by plucking of the hard silica-fume agglomerates during cutting. The paste was typically carbonated around air voids and microcracks, and patchy carbonation was observed throughout the grout. Microcracks were infrequent, narrow, and empty (figure 77). Fragmental carbonate particles up to 0.02 inch long were the principal aggregates in the grout, estimated at 55 to 65 percent by volume (figure 78). Quartz aggregate particles made up approximately 1 to 2 percent of the aggregate. Aggregate distribution was generally uniform. No evidence of deleterious behavior was observed.

The paste contained silica-fume agglomerates, estimated at 1 to 2 percent by volume of paste; residual unhydrated and partially hydrated portland cement particles, estimated at 6 to 8 percent by volume of paste; and calcium aluminate cement (CAC) particles, estimated at 2 percent by volume of paste (figure 79).

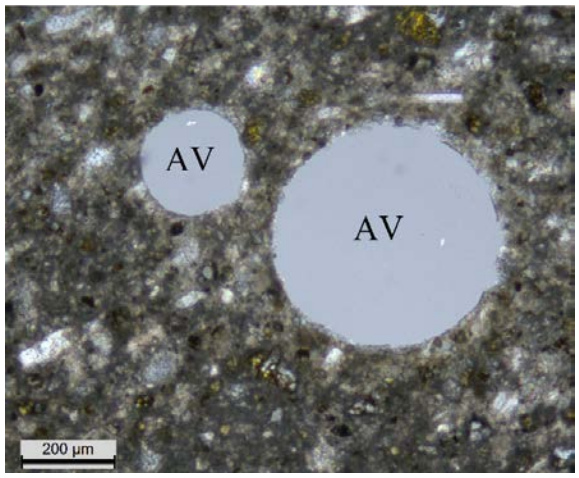

Source: FHWA.

Figure 75. Photo. Thin-section micrograph of Sample #1 P3-2M showing empty, unlined air voids under cross-polarized light with lower polar slightly uncrossed.

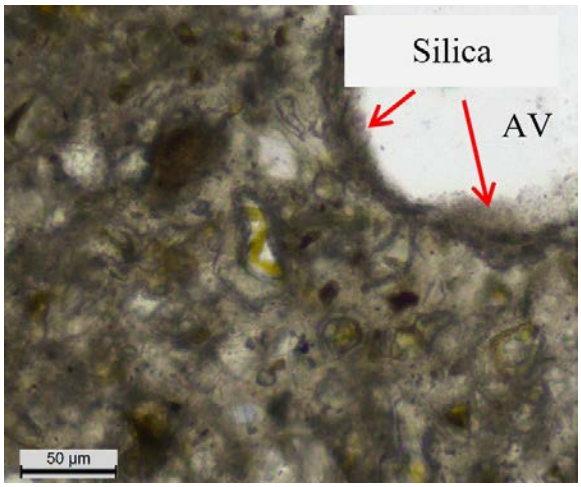

Source: FHWA.

Figure 76. Photo. Thin-section micrograph of Sample #1 P3-2M showing an air void lined with silica fume under plane-polarized light.

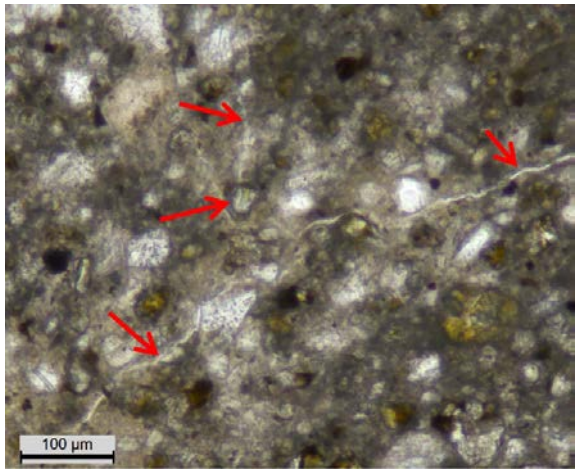

Source: FHWA.

Figure 77. Photo. Thin-section micrograph of Sample #1 P3-2M showing typical microcracks (arrows) under plane-polarized light.

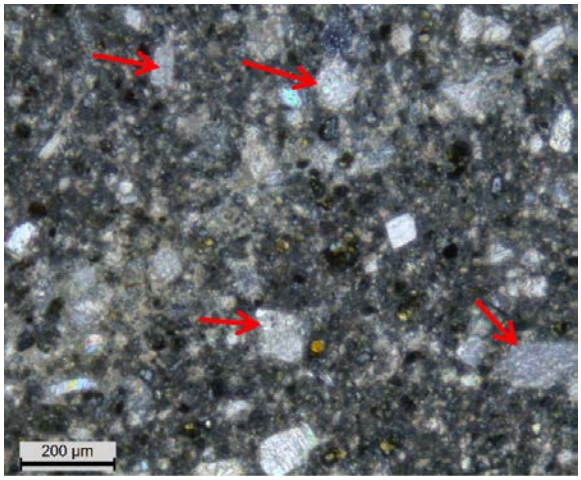

Source: FHWA.

Figure 78. Photo. Thin-section micrograph of Sample #1 P3-2M showing fragmental carbonate aggregates under cross-polarized light.

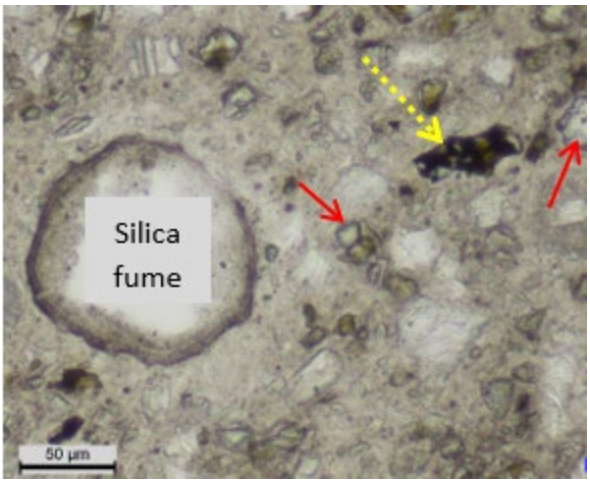

Source: FHWA.

Figure 79. Photo. Thin-section micrograph of Sample #1 P3-2M showing residual portland cement (red solid line arrows) and calcium aluminate cement (yellow dash line arrows) under plane-polarized light.

Sample #1 P3-4 xtra T

The characteristics of the grout in Sample #1 P3-4 xtra T differed in several respects from Sample #1 P3-2M and showed the expected consequences of additional water. Researchers observed regions of hydrated paste that contained few residual cement particles and no aggregate particles (figure 80), but those regions were not abundant. Microcracks were more frequent and tended to be wider (figure 81). The constituents are non-uniformly distributed on a microscale. Overall, the extent of portland cement hydration was higher and many partially hydrated portland cement particles exhibited substantial hydration rims.

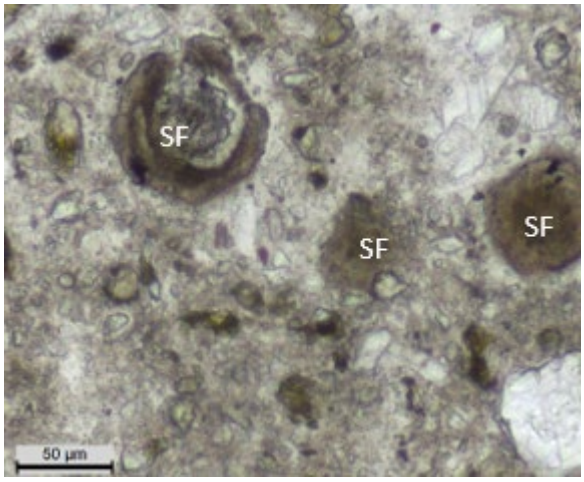

Source: FHWA.

Figure 80. Photo. Thin-section micrograph of Sample #1 P3-4 xtra T showing water-rich regions of paste and silica-fume agglomerates under plane-polarized light.

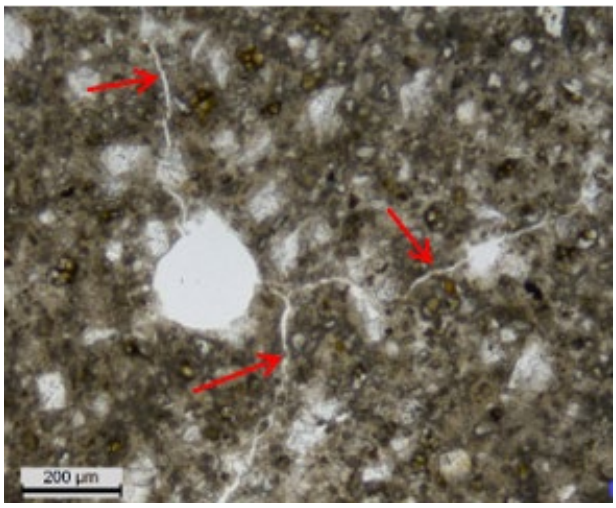

Source: FHWA.

A. Typical shrinkage cracks.

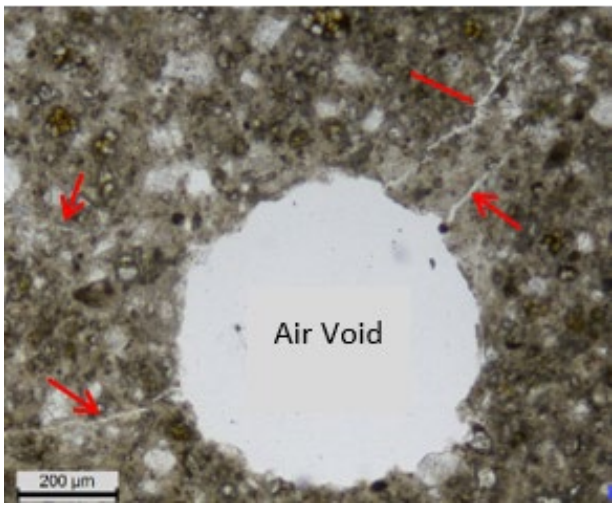

Source: FHWA.

B. Another area showing more shrinkage cracks.

Figure 81. Photos. Thin-section micrographs of Sample #1 P3-4 xtra showing typical shrinkage cracks (arrows) under plane-polarized light.

CHEMICAL ANALYSES

Researchers performed XRD analysis, total sulfur content, and water-soluble sulfate content tests on Sample #1 P3-2M and on the hard and soft portions of the field sample. Total sulfur, reported as percent SO_3 by mass of sample, was determined by evolution and infrared detection. The water-soluble sulfate content of the samples was determined in accordance with ASTM C1580.[(18)] The results are presented in table 14. The crystalline components in the grout samples were determined by XRD. The detectable crystalline components are presented in table 15.

Table 14. Total sulfur and water-soluble sulfate content.

Sample	Total Sulfur as % SO_3 by Mass of Sample	Water-Soluble SO_4, % by Mass of Sample
Sample #1 P3-2M	1.47	0.03
Soft portion of field sample	5.08	3.00
Hard portion of field sample	0.92	0.03

Table 15. XRD results.

Sample	Crystalline Components Detected
Sample #1 P3-2M	Major: Calcite (calcium carbonate), dolomite (calcium magnesium carbonate) Minor: Portlandite (calcium hydroxide) Minor to trace: Ettringite (calcium sulfoaluminate hydrate), larnite (C_2S), calcium silicate (C_3S), biotite (mica)
Soft portion of field sample	Major: Calcite Minor: Ettringite Possibly: Dolomite
Hard portion of field sample	Major: Calcite, dolomite, portlandite Minor to trace: Ettringite Possibly: Gypsum (calcium sulfate dihydrate)

None of the analyzed samples contained a sulfate mineral as a major component. Ettringite was identified as a minor or trace component of each sample and is an expected hydration product of portland cement. Gypsum was identified as a possible trace component of the field sample hard grout.

The total sulfur content of the soft portion of the field sample was more than five times that of the hard portion of the sample and more than three times that of Sample #1 P3-2M. The water-soluble sulfate content of Sample #1 P3-2M and the hard portion of the field sample were the same; however, the water-soluble sulfate content of the soft portion of the field sample was 100 times that of the other samples.

SUMMARY

Researchers examined samples of PTI Class C grout, in both hardened and powder form, using optical microscopy and XRD techniques and tested them for total sulfur and water-soluble sulfate content.

Sample #1 P3-2M and Sample #1 P3-4 xtra T differed in the amount of water used to prepare the grout. Sample #1 P3-4 xtra T, prepared with additional water, exhibited higher paste-to-aggregate ratio and contained more frequent shrinkage cracks compared to Sample #1 P3-2M. Both samples contained fragmental carbonate (identified by XRD as calcite and dolomite), portland cement, silica-fume agglomerates, and a small amount of calcium aluminate cement.

Microscopical examination of the raw grout sample indicated that the recognizable portion (particles larger than approximately 0.197 mil) included 3 to 5 percent anhydrite and a trace amount of gypsum. Particles less than 5 μm also appeared to contain a substantial amount of anhydrite. No large particles of gypsum (calcium sulfate dihydrate) or plaster (calcium sulfate hemihydrate) were observed.

The soft grout field sample contained greater amounts of total sulfur and water-soluble sulfate than either Sample #1 P3-2M or the hard grout field sample. Water-soluble sulfate was concentrated in the pore solutions and, in the segregated grout, sulfate was strongly partitioned into the water-rich portion of the grout, as shown by the analyses of both hard and soft materials from the field sample. The total sulfur content of Sample #1 P3-2M likely represented the actual available sulfur in the grout. The hard grout field sample was depleted in total sulfur (approximately 60 percent of Sample #1 P3-2M), and the soft grout field sample was enriched in total sulfur (approximately 3.5 times). The difference between the samples was not fully explained by the XRD results. Ettringite was detected as a minor component in all three grout samples, which suggests that the source of the sulfate was contained in the fines (particles smaller than 5 μm) of the raw grout powder.

Grout powder contains substantial amounts of particles that are too small to be resolved and identified using optical methods. Sulfate minerals are typically soft and can constitute a major portion of the particles smaller than No. 325 sieve (1.772 mil) when the sulfate mineral is interground with cement clinker, which is substantially harder than sulfate minerals. Researchers can use scanning electron microscopy or energy dispersive X-ray spectroscopy analyses of the raw grout sample to investigate the composition of fine particles that cannot be resolved by

optical microscopy. They can also conduct thermal analyses of the raw samples to quantify the forms of sulfate in the grout.

REFERENCES

1. Freyermuth, C.L. 1991. “Durability of Post-Tensioned Prestressed Concrete Structures.” *Concrete International*, 13 (10): 58-65.

2. ASBI. 2007. *Durability Survey of Segmental Concrete Bridges, 3rd Edition*. Buda, TX: American Segmental Bridge Institute.

3. ASBI. 2012. *Durability Survey of Segmental Concrete Bridges, 4th Edition*. Buda, TX: American Segmental Bridge Institute.

4. Pouliotte, J. 2012. “PT Grouting and Corrosion Issues in Florida.” Presented at the AASHTO T-9 Committee Meeting, Austin, TX.

5. Lau, K. 2014. “Corrosion of Post-Tensioned Tendons in Presence of Deficient Grout.” Presented at FHWA/FDOT Grout Meeting, Gainesville, FL.

6. Lau, K. 2016. *Corrosion of Post-Tensioned Tendons with Deficient Grout*. Report No. BDV 29-977-04. Gainesville, FL: Florida Department of Transportation.

7. Carsana, M. and L. Bertolini. 2015. “Corrosion Failure of Post-Tensioning Tendons in Alkaline and Chloride-Free Segregated Grout: A Case Study.” *Structure and Infrastructure Engineering*, 11 (3): 402-411.

8. CEN. 2007. *EN 445: Grout for Prestressing Tendons – Test Methods.* English Version. Brussels, Belgium: European Committee for Standardization.

9. Carsana, M. and L. Bertolini. 2016. “Characterization of Segregated Grout Promoting Corrosion of Posttensioning Tendons.” *Journal of Materials in Civil Engineering*, 28(6).

10. Korea Institute of Bridge and Structural Engineers and Korea Concrete Institute. 2017. *Tendon Failure Investigation and Follow-up Research Studies, Final Report*. Seoul, South Korea: Seoul Metropolitan Facilities Management Corporation.

11. FHWA. 2013. *Technical Advisory: Recommendations for Assessing and Managing the Long-Term Performance of Post-Tensioned Bridges Having Tendons Installed with Grout Containing Elevated Levels of Chloride.* Washington, DC: Federal Highway Administration. https://www.fhwa.dot.gov/bridge/t514033.pdf, last accessed March 11, 2020.

12. Lee, S-K. and J. Zielske. 2014. *An FHWA Special Study: Post-Tensioning Tendon Grout Chloride Thresholds.* Report No. FHWA-HRT-14-039. Washington, DC: Federal Highway Administration. http://www.fhwa.dot.gov/publications/research/infrastructure/structures/bridge/14039/14039.pdf, last accessed March 11, 2020.

13. Hartt, W.H. and S-K. Lee. 2018. *Corrosion Forecasting and Failure Projection of Post-Tensioned Tendons in Deficient Cementitious Grout*. Report No. FHWA-HRT-17-074. Washington, DC: Federal Highway Administration. https://www.fhwa.dot.gov/publications/research/infrastructure/bridge/17074/17074.pdf, last accessed March 11, 2020.

14. ASTM. 2018. *ASTM A416/A416M-18: Standard Specification for Low-Relaxation, Seven-Wire Steel Strand for Prestressed Concrete.* West Conshohocken, PA: American Society for Testing and Materials International.

15. Lee, S-K. 2012. *Literature Review of Chloride Threshold Values for Grouted Post-Tensioned Tendons.* Report No. FHWA-HRT-12-067. Washington, DC: Federal Highway Administration. https://www.fhwa.dot.gov/publications/research/infrastructure/structures/bridge/12067/12067.pdf, last accessed March 11, 2020.

16. PTI. 2012. *PTI M55.1-12: Specification for Grouting of Post-Tensioned Structures.* Farmington Hills, MI: Post-Tensioning Institute.

17. ASTM. 2014. *ASTM C856-14: Standard Practice for Petrographic Examination of Hardened Concrete.* West Conshohocken, PA: American Society for Testing and Materials International.

18. ASTM. 2015. *C1580-15: Standard Test Method for Water-Soluble Sulfate in Soil.* West Conshohocken, PA: American Society for Testing and Materials International.

HRDI-30/05-21(WEB)E